Dynamical Climatology

Experiments on tropical circulation with a simple moist model.

by

M.K. Davey and A.E. Gill

DCTN 41 June 1986

Meteorological Office (Met. O. 20)
London Road
Bracknell
Berkshire RG12 2SZ

DYNAMICAL CLIMATOLOGY TECHNICAL NOTE NO. 41

EXPERIMENTS ON TROPICAL CIRCULATION WITH A SIMPLE MOIST MODEL

by

M K Davey and A E Gill

Met O 20 (Dynamical
Climatology Branch
Meteorological Office
London Road
Bracknell
Berkshire, U.K. RG12 2SZ

June 1986

Note: This paper has not been published. Permission to quote from it should be obtained from the Assistant Director of the above Meteorological Office branch.

ABSTRACT

A simple model of the circulation of the tropical atmosphere is constructed where the circulation is determined entirely by the sea-surface temperature (SST) pattern, or rather by a forcing field which is closely related to SST. It is an equatorial beta-plane model with an assumed simple baroclinic vertical structure. The moisture and precipitation fields are allowed to evolve freely so there are feedbacks between the latent heating, which contributes to driving the motion, and the low-level velocity field which produces the moisture convergence required to generate precipitation.

Experiments with idealised Pacific SST distributions produce qualitatively realistic precipitation patterns for January (a patch in the west Pacific over the equator) and July (a zonal strip north of the equator).

Analytic solutions for zonally symmetric flow are given to illustrate the basic dynamics and to study the parameter dependence of the precipitation. An analysis of zonal variations shows that a good simplifying approximation for this component is to neglect Rayleigh friction while retaining Newtonian cooling.

The effect of changing the zonal contrast in the prescribed forcing is to gradually alter the circulation from Hadley-like to Walker-like. Along the equator a relatively small contrast is needed to break a zonal band of precipitation.

1. INTRODUCTION

Much of the large-scale tropical circulation is directly driven by heat sources and sinks, so considerable insight into the dynamics follows from a study of the response of an atmosphere to sources and sinks placed near the equator. Simple models with fixed heating have been investigated by, for example, Gill (1980), Lau & Lim (1982), Zebiak (1982), Lim & Chang (1983), Heckley & Gill (1984), Phlips & Gill (1986), all based on linear equatorial beta-plane equations. Webster (1972) has used linear continuous and two-layer models with prescribed heating.

Specifying the heating begs the question of why sources and sinks are located at particular spots, however. In practice, the main sources are due to latent heat release in the troposphere in regions of deep convection. The fuel for such heat sources is the moisture which is carried to the source by a field of motion which itself depends on the strength and location of the source. Understanding the dynamics requires an appreciation of the interdependence between the moisture field and the flow field. In a series of papers, Gill (1982b, 1982c, 1985) has developed the simplest possible model for examining this relationship. A more complex model with active moisture can be found in Lorenz (1984), and the two-level model by Held & Suarez (1978) is a further step toward the full physics of a general circulation model.

The simplicity of the Gill model stems from assuming a fixed

baroclinic structure in the vertical which leads to the linearised shallow-water equations. With this structure, flow in the lower troposphere is oppositely directed to that in the upper troposphere, with zero horizontal velocity at mid-level. The vertical velocity is maximum at mid-level, as are thermal perturbations produced by heating. Simplicity in the moisture equation comes from the assumption that moisture is confined to the lower troposphere, so the moisture flux is determined by the low-level winds and the total column moisture Thus the full set of equations consists of the shallow-water equations plus a dynamic moisture equation and a condition (namely that a saturation level is reached) for precipitation and latent heat release. The equations involve only horizontal position and time, as vertical structure is specified.

The model needs some representation of the forcing which would occur even in the absence of latent heat release. In particular, a simple representation is required of the heating that takes place due to the sun shining on the ocean and setting off the chain of processes that determines the sea surface temperature (SST) and the structure of the atmosphere above it. In the simple model this heating can only be represented by a source term in the thermal equation. This term defines a temperature Θ_s towards which the mid-level temperature perturbation θ is driven. The equations are linearised about a state of rest with uniform horizontal stratification.

The purpose of this paper is to determine the response of the

moist model for different prescribed fields of θ_s. For instance, what properties of the θ_s distribution determine whether the response circulation is predominantly Hadley-like or Walker-like? For answering such questions the precise relationship between θ_s and fields one might observe is not important. However, it is clear that θ_s will be closely related to SST, i.e. that there are thermal processes which will tend to make the mid-level temperature field in the tropics vary with latitude and longitude in a similar way to the surface field. For instance, a constant lapse rate between the surface and mid-levels would require the two fields to be identical. In a numerical experiment by Rowntree (1976) using a general circulation model of the atmosphere with a specified SST anomaly, a direct relation between mid-level heating and SST was apparent.

Following a detailed presentation of the model equations in section 2, we examine in section 3 the response to θ_s distributions based on observed SST fields for the tropical Pacific Ocean, for January and July conditions. Circulation and precipitation patterns quite like actual ones are found.

In sections 4 and 5 some simple examples are examined for zonally symmetric flow with and without precipitation, showing how latent heat release intensifies and narrows regions of upward motion. The dependence of precipitation location and magnitude on the saturation moisture level is also examined analytically. Departures from zonal symmetry are similarly treated in sections 6 and 7. We find that it is a good approximation to neglect Rayleigh friction while retaining

Newtonian cooling in the dynamics of zonally-varying flow. A method of estimating precipitation is given in section 7. The influence of zonal variations on precipitation patterns is discussed further in section 8, with reference to Hadley-type and Walker-type circulation.

2. THE MODEL AND THE GOVERNING EQUATIONS

2.1 Vertical structure and nondimensional equations

There are various ways of deriving the model equations, based on different formulations of the vertical structure. For the purposes of this paper it seems best to use the simplest one, with the atmosphere incompressible and bounded by rigid horizontal planes at $z^* = 0$ and $z^* = \pi H$. The velocity (u^*, v^*, w^*) and potential temperature change Θ^* are small perturbations from a state of rest with constant buoyancy frequency N given by

$$N^2 = \frac{g}{\Theta_0} \frac{d\Theta}{dz^*} \qquad (2.1)$$

Here g is the acceleration due to gravity and Θ is the undisturbed potential temperature with characteristic value Θ_0.

Equations are derived for an equatorial beta-plane, where β^* is the gradient of the Coriolis parameter at the equator, x^* is distance eastward, and y^* is distance northward from the equator. Horizontal velocity is scaled by the maximum internal gravity wave speed

$$C = NH \quad , \qquad (2.2a)$$

and horizontal distance is scaled by the equatorial Rossby radius

$$a = (C/2\beta^*)^{\frac{1}{2}} \qquad (2.2b)$$

with corresponding timescale

$$\tau = a/C \ . \qquad (2.2c)$$

The typical speed C = 50 m sec gives a Rossby radius of 1000 Km and a timescale of a quarter of a day. Non-dimensional independent variables are

$$x = x^*/a \ , \ y = y^*/a \ , \ z = z^*/H \ , \ t = t^*/\tau. \qquad (2.3)$$

For the dependent variables, vertical structure and non-dimensional form are

$$(u^*, v^*) = (u, v)\ C \cos z \qquad (2.4a)$$

$$w^* = w\ (CH/a) \sin z \qquad (2.4b)$$

$$\Theta^* = \Theta\ (N\Theta_0 C/g) \sin z \qquad (2.4c)$$

Thus u and v represent low-level horizontal velocity, whereas w and Θ represent mid-level values --- see Fig. 1. Note that

$$N\Theta_0 C/\varepsilon = \frac{d\Theta}{dz^*} H \ ,$$

so the scale for θ^* is the difference in the static value Θ over height H.

Substitution of these forms into the linear horizontal momentum and temperature equations and the incompressibility condition leads to, after use of the hydrostatic equation,

$$u_t - fv = \Theta_x - \varepsilon u + \nu\nabla^2 u \qquad (2.5)$$

$$v_t + fu = \Theta_y - \varepsilon v + \nu\nabla^2 v \qquad (2.6)$$

$$\Theta_t + w = \varepsilon(\Theta_s - \Theta) + \nu\nabla^2\Theta + Q \qquad (2.7)$$

$$u_x + v_y + w = 0 \qquad (2.8)$$

where

$$f = \beta y \qquad \text{with} \qquad \beta = \frac{1}{2} \qquad (2.9)$$

(See Gill 1980 for details). These equations include Raleigh friction with dimensional decay time τ/ε , and Newtonian cooling with the same time-scale for convenience. Laplacian dissipation and diffusion with coefficient ν is used in some numerical experiments, as described later. In the absence of vertical motion Θ is forced

towards a fixed temperature distribution θ_s which is assumed to have the same pattern as the underlying sea-surface temperature (SST). The remaining term Q in (2.7) represents latent heating, which is related to moisture as described below.

The moisture budget takes a simple form when we assume that the scale height of the moisture distribution is small compared with H. Then the moisture flux is

$$\int \underline{u}^* s^* dz^* = C \, \underline{u} \, q^* \tag{2.10}$$

where s^* is specific humidity and

$$q^* = \int s^* dz^* \tag{2.11}$$

is the total column moisture with units of Kg m-2. The dimensional moisture equation is

$$\frac{\partial q^*}{\partial t^*} + C \left[\frac{\partial (uq^*)}{\partial x^*} + \frac{\partial (vq^*)}{\partial y^*} \right] = E^* - P^* + \text{diffusion} \tag{2.12}$$

where E^* and P^* represent evaporation and precipitation. When $P^* > 0$ there is latent heat release, giving a heating rate

$$Q^* = \frac{\rho_w L}{\rho_a c_p 2H} P^* \tag{2.13}$$

where ρ_w and ρ_a are water and air densities, c_p is the specific heat of air, and L is the latent heat of vaporisation of water. The factor 2H is obtained when the latent heat release drives only the vertical structure defined in (2.4). The scales defined earlier relate Q and Q^* by

$$Q^* = (N\Theta_0 C/g\tau)\, Q \qquad (2.14)$$

It is useful to similarly scale q^* and P^* by

$$q^* = \frac{\rho_a c_p 2H}{\rho_w L} \frac{N\Theta_0 C}{g} q \quad , \qquad (2.15a)$$

$$P^* = \frac{\rho_a c_p 2H}{\rho_w L} \frac{N\Theta_0 C}{g\tau} P \quad . \qquad (2.15b)$$

Then (2.13) reduces to

$$Q = P \qquad (2.16)$$

and the moisture equation (2.12) becomes

$$q_t + (uq)_x + (vq)_y = \varepsilon(\hat{q}-q) + \nu\nabla^2 q - P \quad . \qquad (2.17)$$

In this equation evaporation is assumed to push q toward some saturation value $\hat{q}$: for simplicity the rate of this process is

chosen to be the same as for Raleigh friction and Newtonian cooling.

We require that q never exceeds some threshold value, taken here to be simply $\hat{q}$. Let

$$R = - (uq)_x - (vq)_y + \xi(\hat{q}-q) + \nu\nabla^2 q \quad . \tag{2.18}$$

If at any time R is positive and q has reached $\hat{q}$ then it rains, because there is a tendency to drive q above $\hat{q}$. All excess moisture is precipitated, so

$$P = R = - (u\hat{q})_x - (v\hat{q})_y + \nu\nabla^2 \hat{q} \tag{2.19}$$

when

$$R > 0 \quad \text{and} \quad q = \hat{q}.$$

Otherwise it does not rain, in which case

$$P = 0 \ , \ q_t = R. \tag{2.20}$$

Further discussion of this moisture budget can be found in Gill (1982a).

The quantity $\hat{q}$ plays a very important role in determining the behaviour of the system. This can be seen by considering the case where $\hat{q}$ is everywhere constant and (2.17) is linearised to become

$$q_t - \hat{q} w = \xi(\hat{q}-q) - P + \nu\nabla^2 q \quad . \tag{2.21}$$

Then in a region of rain we have

$$P = \hat{q}w \tag{2.22}$$

and the temperature equation (2.7) can be written

$$\theta_t + (1-\hat{q})\, w = \varepsilon(\theta_s - \theta) + \nu\nabla^2\theta \quad . \tag{2.23}$$

The form of this equation is the same as in the dry case, except that the buoyancy restoring term w in (2.7) is replaced by $(1-\hat{q})w$ in (2.21). The difference arises because the latent heat release opposes the reduction of buoyancy due to adiabatic vertical motion, so the buoyancy restoring force is reduced. Note that when $\hat{q}=1$, latent heating and adiabatic cooling effects cancel exactly.

The effect of this buoyancy reduction was examined in Gill (1982a) and many interesting phenomena were found, such as propagating fronts and rainbands whose characteristics depend on the value of $\hat{q}$. Features propagate at unit speed in non-precipitating regions, but at speed $(1-\hat{q})^{\frac{1}{2}}$ in regions of rain. For the large-scale tropical circulation problems studied in following sections we take $\hat{q} = 8/9$ (unless otherwise specified), so the latter speed is 1/3.

If $\hat{q} > 1$ then the term $(1-\hat{q})w$ in (2.23) is not a restoring effect, and the system is locally unstable. This state corresponds

to the vertical potential temperature gradient being moist unstable. Some solutions for a uniformly rotating atmosphere with $\hat{q} > 1$ were discussed in Gill (1982b), corresponding to hurricane-like disturbances. The size of these features is governed by a "moist Rossby radius" equal to $(\hat{q}-1)^{\frac{1}{2}}$ times the dry value. (Likewise there is a reduced "moist Rossby radius" $(1-\hat{q})^{\frac{1}{2}}a$ for the stable case $\hat{q} < 1$.) Equatorial solutions with $\hat{q}>1$ can be seen in Davey (1985): for $\hat{q}$ just greater than 1 advection and diffusion stabilise the circulation, but for larger $\hat{q}$ disturbances were found to grow and decay irregularly.

Solutions of the equations on an equatorial beta-plane have been discussed in Gill (1985): in particular a zonally-symmetric solution with a feature corresponding to the Inter - Tropical Convergence Zone was obtained. As $\hat{q}$ tends to one from below the width of the zone shrinks to zero but the precipitation rate increases correspondingly. An analytic solution was obtained for the case $\hat{q} = 1$.

2.2 Steady equations

From section 4 on we will mainly consider the steady linearised equations with constant $\hat{q}$. Neglecting Laplacian terms these are written

$$-fv = \theta_x - \varepsilon u \tag{2.24}$$

$$fu = \theta_y - \varepsilon v \tag{2.25}$$

$$\alpha w = \varepsilon(\theta_s - \theta) \tag{2.26}$$

where

$$\alpha(x,y) = \begin{cases} 1 & \text{no precipitation} \\ 1 - \hat{q} & \text{precipitation} \end{cases} \tag{2.27}$$

In terms of θ, we have

$$u = (\varepsilon\theta_x + f\theta_y) / (\varepsilon^2 + f^2) \tag{2.28a}$$

$$v = (\varepsilon\theta_y - f\theta_x) / (\varepsilon^2 + f^2) \tag{2.28b}$$

and an equation for θ alone is

$$\alpha[-\varepsilon(\varepsilon^2+f^2)\nabla^2\theta + (\varepsilon^2 - f^2)\beta\theta_x + \varepsilon f\theta_y] = \varepsilon(\varepsilon^2+f^2)^2(\theta_s - \theta) \tag{2.29}$$

In view of the boundary conditions to be used, i.e. $v = 0$ at northern and southern "walls", it is often more convenient to solve the equation for v alone:

$$\alpha[\varepsilon\nabla^2 v + \beta v_x] - \varepsilon(\varepsilon^2+f^2)v = \varepsilon f\theta_{sx} - \varepsilon^2\theta_{sy} . \tag{2.30}$$

Although equations (2.29) and (2.30) are linear in either the rain or no-rain regions separately, they are non-linear regarding the position of the rain/no rain boundary, and must usually be

solved using numerical methods. Once v and Θ_s are known, u and θ can be found latitude-by-latitude using

$$\alpha u_{xx} - \varepsilon^2 u = -\alpha v_{xy} - \varepsilon \Theta_{sx} - f \varepsilon v \quad , \tag{2.31}$$

$$\alpha \Theta_{xx} - \varepsilon^2 \Theta = -\alpha f v - \varepsilon^2 \Theta_s - \alpha \varepsilon v_y \quad . \tag{2.32}$$

Another useful equation obtained from the curl of (2.24) and (2.25) is

$$-\beta v + f w = \varepsilon (v_x - u_y) \tag{2.33}$$

which for vanishing Rayleigh friction reduces to the Sverdrup relation

$$\beta v = f w \quad . \tag{2.34}$$

We shall see later that (2.34) is a good approximation for the zonally-varying component of flow, and it means that upward motion is accompanied by poleward low-level flow.

From (2.21), the steady moisture field is (neglecting diffusion)

$$q = \begin{cases} \hat{q} & \text{rain} \\ \hat{q}\,(1 + w/\varepsilon) & \text{no-rain} \end{cases} \tag{2.35}$$

Some general statements can be made about the location of precipitation. From (2.35), it must rain where $w > 0$. Then from

(2.26) we deduce

$$\begin{aligned} w < 0 \quad &\Rightarrow \quad \theta > \theta_s \qquad \text{no rain} \\ w = 0 \quad &\Rightarrow \quad \theta = \theta_s \qquad \text{rain/no-rain boundary} \\ w > 0 \quad &\Rightarrow \quad \theta < \theta_s \qquad \text{rain} \end{aligned} \tag{2.36}$$

The constraint that there be zero net vertical motion requires $w > 0$ somewhere (except in the static $w \equiv 0$ case), so in this steady model it must rain somewhere, but not everywhere.

From (2.29) we find that θ_s must be greater than θ wherever θ has a local maximum, so it must rain at such a point. Physically this location is a low pressure centre, associated with low-level convergence and rising motion. Further, we can deduce that the absolute maximum of θ_s must lie inside a region of precipitation.

It is sometimes useful to write (2.26) in another form, by defining a latent-heating temperature

$$\theta_L = P/\varepsilon = \begin{cases} \hat{q}\, w/\varepsilon = (\theta_s - \theta)\, \hat{q}/(1-\hat{q}) & \text{rain} \\ 0 & \text{no rain} \end{cases} \tag{2.37}$$

to give

$$w = \varepsilon(\theta_s + \theta_L - \theta) \,. \tag{2.38}$$

Thus the solution of the model with rain and forcing θ_s can be expressed as the <u>linear</u> superposition of models with no rain and forcing θ_s and θ_L . Generally θ_L is not known a priori, but, as described later, θ_L can be parameterised to obtain estimates of solutions with rain.

2.3 Energy equation.

Although we shall not have cause to refer to it, we state here for completeness the energy equation for the simple model. When q is constant it is useful to define a new variable "dryness"

$$d = 1 - q / \hat{q} \tag{2.39}$$

which is zero for saturated air and unity for completely dry air. From (2.17),

$$d_t + w + \nabla_{\cdot}(\underline{u} d) = \nu \nabla^2 d - \varepsilon d + P/\hat{q} \tag{2.40}$$

with $d_t = 0$ where precipitation occurs. The basic equations (2.5) to (2.8), (2.40) lead to

$$\overline{\overline{e}}_t = \hat{q}\,\overline{\overline{(\theta-\alpha)\nabla_{\cdot}(\underline{u}\alpha)}} - \nu\left\{(1-\hat{q})\overline{\overline{[(\nabla w)^2+(\nabla v)^2+(\nabla\theta)^2]}} + \hat{q}\,\overline{\overline{[\nabla(\theta-\alpha)]^2}}\right\} - 2\varepsilon\,\overline{\overline{e}} + \varepsilon\,\overline{\overline{\theta_s[(1-\hat{q})\theta + \hat{q}(\theta-\alpha)]}} \tag{2.41}$$

where

$$e = \tfrac{1}{2}\left[(1-\hat{q})(u^2+v^2+\theta^2) + \hat{q}(\theta-d)^2\right] \tag{2.42}$$

is a positive definite quantity for $\hat{q}<1$, and the double overbar denotes an average over the entire area of flow. Precipitation has been explicitly eliminated in deriving (2.41), partly by using the identity

$$Pd = 0 \quad . \tag{2.43}$$

(Either it is raining, so d = 0, or it is not raining and P = 0.) When $\hat{q}=0$ then (2.42) is the usual sum of kinetic and potential

energy.

If the nonlinear term $\nabla_z (\underline{v}d)$ is omitted from (2.40) then the first term on the right-hand side of (2.41) does not appear. The second and third terms are negative, and the fourth term contains the only forcing via θ_s. In the absence of forcing a system with $\hat{q}<1$ must tend to a steady state with $u = v = \theta = d = 0$.

3. RESULTS FOR "JANUARY" AND "JULY" SIMULATIONS FOR THE PACIFIC

The simple model was constructed as a means of improving understanding of moisture effects on the large-scale circulation in the tropics, so can it produce reasonable precipitation fields for the Pacific Ocean?

The model is for flow over the ocean only, and requires a sea surface temperature pattern as input. To achieve this, an equatorial beta-plane channel was set up with boundaries at $y = \pm 4$ (about 40° latitude) and with periodic east-west boundary conditions — effectively a periodically repeated Pacific Ocean with no land or other oceans in between. The length of the model Pacific is 16 units (about 160° longitude). The forcing temperature Θ_s was set by specifying a western meridional profile $\Theta_W(y)$ to apply at $x = -4$, and an eastern profile $\Theta_E(y)$ for $x = +4$, with periodic behaviour in between:

$$2\,\Theta_s = \Theta_E + \Theta_W + (\Theta_E - \Theta_W)\sin(\pi x/8) \qquad (3.1)$$

The eastern and western profiles were chosen by constructing analytic curves with similar properties to the observed ones. For the western Pacific,

$$\Theta_W = 1 - (y-Y)^2\,(Y^2+2yY+16) \,/\, (Y^2-16)^2 \qquad (3.2)$$

with $Y = 0$ for January and $Y = 1.5$ for July. This curve vanishes at

the channel boundaries $y = \pm 4$ and has a maximum of one at y=Y. The eastern profile is

$$\Theta_E = 0.6\ (1-y^2/16) + A \exp\{-(y-1)^2\} \qquad (3.3)$$

with A = 0.1 for January and A = 0.3 for July. The first term in (3.3) gives a parabolic shape vanishing at $y = \pm 4$ and with a maximum of 0.6 at the equator. The second term adds a Gaussian bump centred at y = 1. Overall, the maximum eastern value is 0.67 in January and 0.87 in July.

Eqs. (2.5)-(2.7), (2.17) were solved by numerical integration, time-stepping on a finite-difference spatial C-grid with spacing of half a Rossby radius in each direction. To ensure numerical stability Laplacian diffusion of u,v,Θ and q was included. Results are shown for the parameter values $\hat{q} = 8/9$, $\varepsilon = 0.1$, and $\nu = 0.025$. Integration is carried out to t = 60, by which time the response is effectively steady. (Diagrams for $\hat{q} > 1$ can be seen in Davey (1985) and Gill (1985).)

Fig. 2 shows the temperature patterns Θ_s that force the motion. Perturbation mid-level potential temperature Θ, low-level velocity, dryness $d = 1-q/\hat{q}$ and precipitation rate P appear in Figs. 3-6 for January and July.

In January the forcing field is characterized by having the maximum temperature on the equator in the west, with a relatively large east-west temperature contrast (0.33 difference between eastern and western maxima). As expected, the rainfall is centred over the warmest ocean, thereby giving a response like the winter

monsoon with heavy precipitation over the Indonesian region. The precipitation rate is similar in magnitude to $\epsilon \Theta_s$, so latent heating and heating by Θ_s are comparable. The driest regions, which mark the zones of maximum downward motion, are an extensive area on the eastern side south of the equator, and a less extensive area on the eastern side north of the SST maximum. The moister zone has a narrow westward extension along the equator from its centre over Indonesia, and broader extensions on the east to both the north-east and south-east. The south-east extension is a sharper feature which can be related to the South Pacific Convergence Zone. The main contrasts are between east and west, giving the impression of a Walker-cell type of structure.

In July the forcing field is rather different, with maximum values in the northern hemisphere near y = 1. Precipitation is again found over the warmest ocean, but is now very elongated east-west to form an extensive Inter-Tropical Convergence Zone. The driest area in the tropics is now at the same longitude as the warmest water, in the west, but located in the opposite hemisphere to the precipitating region. Thus a Hadley-like circulation is apparent with rising motion over the warmest water and a descending branch in the southern hemisphere.

The low-level winds are dominated by easterly trade winds off the equator, being associated with the thermal wind due to the north-south temperature gradient. In January the trades extend right across the equator in the central Pacific, where they reach their strongest values and constitute the low-level branch of the Walker circulation. To the west of Indonesia there are very strong westerly

monsoon winds directed into the zone of heavy precipitation.

In July the southern hemisphere trades are strongest and there is a marked cross-equatorial flow, particularly in the west, providing the low-level branch of the Hadley cell. This flow veers strongly as it crosses the equator and becomes westerly in the northern hemisphere. There is a region of very weak flow at about 15° N ($y = 1.5$) where a very shallow trough separates these westerlies from the easterlies further north.

The maps of mid-level potential temperature perturbation θ are relatively featureless, showing much less zonal contrast than θ_s and with no clear indication of precipitation regions. Maps of vertical velocity (not shown) are dominated by strong ascent where it is raining, with much weaker downward motion elsewhere.

Obviously a simple model like the one described will not give a perfect simulation of observation, but the patterns are very much like real ones and this encourages the belief that ideas stemming from further analysis will be useful for understanding the real atmosphere. With the model it is easy, for example, to vary east-west contrasts in the forcing SST field to see at what point Walker cell characteristics start to become more pronounced than those of a Hadley cell. Analysis can be done to determine the relative magnitudes of various processes, etc. The remainder of the paper will be devoted to such questions, beginning with the simplest case of zonally symmetric flow.

4. ZONALLY SYMMETRIC STEADY SOLUTIONS: DRY CASE

When no rain is allowed in the model and there is no east-west variation, some useful simple solutions can be obtained. In this case the steady equation (2.30) for v reduces to

$$v_{yy} - (f^2 + \varepsilon^2)\, v = -\varepsilon \theta_{sy} \tag{4.1}$$

where $f = y/2$. In terms of v other variables are

$$u = fv/\varepsilon \tag{4.2}$$

$$w = -v_y \tag{4.3}$$

$$\theta = \theta_s + v_y/\varepsilon \ . \tag{4.4}$$

Eq. (4.1) can be easily solved numerically in any given case. The term ε^2 is usually small: certainly for $\varepsilon \lesssim 0.1$ results with this term neglected are almost identical to those with ε^2 retained. Hence we shall use the approximate equation

$$v_{yy} - f^2 v = -\varepsilon \theta_{sy} \tag{4.5}$$

which has analytic solutions. With $\theta_s \sim 1$, the ordering of the dependent variables is

$$v \sim \varepsilon \ , \quad w \sim \varepsilon \ , \quad \theta \sim 1 \ , \quad u \sim 1 \ .$$

As an archetype of the behaviour to be expected, an analytic solution can be found when the surface temperature has the parabolic shape

$$\Theta_s = 1 - (y/b)^2 \quad . \tag{4.6}$$

A particular solution of (4.5) with $v \to 0$ as $|y| \to \infty$ is

$$v = - (8\varepsilon/b^2)\, \hat{P}(y) \quad . \tag{4.7}$$

Here

$$\hat{P}(y) = \frac{\hat{a}\, y}{2} \sum_{n=0}^{\infty} A_n (y^4/4)^n - \frac{y^3}{4} \sum_{n=0}^{\infty} B_n (y^4/4)^n \tag{4.8}$$

with

$$A_0 = 1 \quad , \qquad A_n = A_{n-1} /(4n+1)4n$$

$$B_0 = 1/6 \quad , \qquad B_n = B_{n-1} /(4n+3)(4n+2)$$

$$\hat{a} = (\pi/2)^{3/2} \; [\, 2\,\Gamma(5/4)\,]^{-2} \approx 0.59907$$

This function $\hat{P}$ is well-known in oceanography as the solution for a "Yoshida Jet", which is illustrated in Fig. 11.14 of Gill (1982a). Mathematically, $\hat{P}/y^{\frac{1}{2}}$ is a Lommel function of order 1/4 and argument $y^2/4$.

If we impose the condition v = 0 at the channel walls at $y = \pm b$ then free solutions of (4.5) must be added. It is convenient to use the odd and even free solutions (Abramowitz & Stegun 1970, section 19)

$$Vo(y) = y \sum_{n=0}^{\infty} A_n \, (y^4/4)^n \tag{4.9a}$$

$$Ve(y) = \sum_{n=0}^{\infty} C_n \, (y^4/4)^n \tag{4.9b}$$

With A_n as above, and

$$C_0 = 1 \quad , \qquad C_n = C_{n-1} / 4n(4n-1) \quad .$$

These solutions have

$$Vo = 0 \ , \ dVo/dy = 1 \ , \ Ve = 1 \ , \ dVe/dy = 0 \quad \text{at} \quad y=0 \ .$$

Then the solution with v vanishing on the channel walls is

$$v = -\varepsilon F(y) \tag{4.10a}$$

where

$$F(y) = (8/b^2) \left[\hat{P}(y) - Vo(y) \, \hat{P}(b) / Vo(b) \right] \quad . \tag{4.10b}$$

Profiles of u,v,w and θ for the case $b = 4$ are shown in Fig. 7, along with streamlines and normal flow in a meridional section. There are low-level easterly jets north and south of the equator, with u vanishing at the equator as required by (4.2). Meridional flow is equatorward at low-level, giving broad rising motion around the equator.

Another useful case to consider is the response to forcing at one latitude only, i.e. for the heat source

$$\theta_s = \delta(y-y_0) \quad . \tag{4.11}$$

Then the solution to (4.5) with $v = 0$ at $y = \pm b$ is

$$v = \quad -\varepsilon H_y(-y_0) \, H(y) / W \qquad y_0 < y \leq b \ ,$$

$$v = \qquad (4.12)$$

$$\varepsilon H_y(y_o)\, H(-y) / W \qquad -b \leq y < y_o$$

where

$$H(y) = Ve(y) - Vo(y)Ve(b)/Vo(b),$$

and

$$W = H_y(y_o)\, H(-y_o) + H(y_o)\, H_y(-y_o) = -2\, Ve(b)/Vo(b)$$

is a Wronskian whose value is independent of y_o. The potential temperature is

$$\Theta = \begin{cases} -H_y(-y_o)\, H_y(y) / W & y_o \leq y \leq b \\ -H_y(y_o)\, H_y(-y) / W & -b \leq y \leq y_o \end{cases} \qquad (4.13)$$

and vertical velocity is simply

$$w = -\varepsilon \Theta \qquad \text{for } y \neq y_o . \qquad (4.14)$$

Profiles of u, v, and Θ are given in Fig. 8 for $y_o = 0$ and $y_o = 1$. As we would expect, low-level flow is toward the heat source, with a discontinuity at y. Except for the case $y_o = 0$, there is a corresponding discontinuity in the zonal flow, with westerlies between y_o and the equator, and easterlies elsewhere. The discontinuity in u follows from the discontinuity in v, due to the balance of damping and Coriolis terms as described by (4.2). Temperature is positive and continuous everywhere, and w is negative everywhere except at $y = y_o$ where there is a positive spike such that there is zero net vertical velocity. (Circulation in a meridional plane can be seen in Fig. 11.18 of Gill (1982a) for a similar example.) The strength of the upward motion, which is related to the discontinuity in v at y_o, is proportional to the

strength of the heat source. Note that the strongest downward motion is adjacent to y_0.

5. ZONALLY SYMMETRIC STEADY SOLUTIONS: MOIST CASE

When precipitation is allowed the problem is more difficult to solve because the boundary of the region of rain is not known beforehand. The most general and straightforward method of solution is to numerically integrate the time-dependent equations to a steady state, as in section 3. Some analytic progress can be made for simple cases, however, and this approach is described below because it gives information about how the location and amount of precipitation depends on various parameters.

The basic equation is the zonally-symmetric form of (2.30):

$$\alpha\, v_{yy} - (\ell^2 + f^2)\, v = -\ell\, \theta_{sy} \tag{5.1}$$

where $\alpha = 1$ (no rain) or $1-\hat{q}$ (rain). We restrict attention to moist stable cases with $\hat{q}<1$ so α is positive. Other velocity components u and w can be obtained using (4.2)-(4.3), while (4.4) is modified to

$$\theta = \theta_s + \alpha\, v_y / \ell \ . \tag{5.2}$$

Once w is known, the moisture field can be found from (2.35).

For the zonally-symmetric case net precipitation per unit zonal distance in a rainband is related to v by

$$P_{TOT} = \int P\, dy = \hat{q} \int_{y_-}^{y_+} w\, dy$$
$$= -\hat{q}(v_+ - v_-) \tag{5.3}$$

where subscripts + and - denote the northern and southern edges of the rainband. Motion is upward in this region, so v_+ must be less than v_- to provide the required low-level convergence.

As described in section 2, rain must occur over the location y_0 of the maximum θ_{s0} of θ_s, and as $\hat{q}$ approaches unity the region of rain shrinks to this point. Hence as a first estimate we suppose it only rains at y_0, so $y_- = y_0 = y_+$. (Only one maximum of θ_s will be considered: the extension to multiple equal maxima giving double ITCZ-like structures follows the same method). Vertical velocity vanishes at the rain/no-rain boundary, so the dry equation (4.5) can be solved in the region $-b < y < y_0$ with

$$v = 0 \qquad \text{at } y = -b$$

$$v_y = 0 \qquad \text{at } y = y_- \quad , \tag{5.4a}$$

and in $y_+ < y < b$ with

$$v = 0 \qquad \text{at } y = b$$

$$v_y = 0 \qquad \text{at } y = y_+ \quad . \tag{5.4b}$$

The solution gives values for v_- and v_+, and hence an estimate for the net precipitation (5.3). For example, with the parabolic profile (4.6) for θ_s

we have $y_0 = 0$ and find

$$v = -\varepsilon [\, F(y) - H(y)\, F_y(0) / H_y(0) \,] \tag{5.5}$$

for $0 < y \lesssim b$, with opposite sign for $y<0$. The functions F and H were defined in (4.10) and (4.12). Thus

$$v_+ = \varepsilon F_y(0) / H_y(0) \qquad (5.6)$$
$$= - v_-$$

For $b = 4$ the precipitation estimate is

$$P_{TOT} = -2\hat{q}v_+ = 0.61\,\varepsilon\hat{q} \qquad (5.7)$$

which will later be compared with exact values (see Fig. 10).

The expression (5.5) is simply a linear superposition of solutions obtained in section 4 for parabolic Θ_s and for a point source on the equator. The rainfall can be regarded as providing an extra heating term as described in section 2 with, in this case, known position but magnitude to be determined by the condition $w = 0$ at the rain/no-rain boundary. For the point source, this condition is equivalent to requiring

$$\Theta = \Theta_s \text{ at } y_0 .$$

To improve this initial estimate we allow the rainfall band to have finite width. One method is to match solutions in regions with and without precipitation. For parabolic Θ_s, solving the dry equation (4.5) with boundary condition (5.4) gives for the northern no-rain region

$$v(y) = - \varepsilon[\, F(y) - H(y)\, F_y(y_+) / H_y(y_+) \,] \quad , \qquad (5.8)$$

with a similar expression for the southern region. In Fig. 9 the graph of $v_+ = v(y_+)$ as a function of y_+ shows that the magnitude of

v_+ decreases as y_+ increases (v_- behaves in the same way), so allowing finite width decreases the net precipitation. In the wet region centred on y_0 we approximate (5.1) by

$$(1-\hat{q})v_{yy} = -\mathcal{E}\,\theta_{sy} \,, \tag{5.9}$$

This approximation can be shown to be valid in the limit of small $(1-\hat{q})$. Integrating twice for parabolic θ_s, using symmetry and requiring $v_y = 0$ at y_+ leads to

$$(1-\hat{q})v = \mathcal{E}\, y(y^2 - 3y_+^2) \,/\, 3b^2 \,. \tag{5.10}$$

In particular,

$$v_+ = -2\mathcal{E}\, y_+^3 \,/ 3b^2(1-\hat{q}) \,. \tag{5.11}$$

Matching with (5.8) gives an equation to solve for y_+. (Note that y_+ is independent of $\mathcal{E}$.) For small y_+ the approximate value of v_+ is given by (5.6): with this value an explicit estimate of y_+ is

$$y_+^3 = -3b^2(1-\hat{q})\, F_y(0) \,/\, 2H_y(0) \tag{5.12}$$

which for $b = 4$ is

$$y_+ = 1.94\,(1-\hat{q})^{1/3} \,. \tag{5.13}$$

Estimates obtained by matching (5.11) with (5.8) are shown in Fig. 10 for various values of $\hat{q}$, along with exact values found by solving (5.1) numerically. The prediction is quite good, even for wide rainbands. Precipitation is overestimated and the width of the rainband is increasingly underestimated as $\hat{q}$ decreases and rainband

width increases. Exact y_+ values are closely proportional to $(1-\hat{q})^{1/3}$.

For $\hat{q} = 8/9$, profiles of u, v, w and θ obtained numerically with $\varepsilon = 0.1$ are shown in Fig. 11. Compared to the dry case in Fig. 7, we see that larger upward motion occurs over a narrower region when latent heating is included; this effect becomes more pronounced as $\hat{q}$ approaches unity.

Note that θ is almost constant in the region of precipitation. A second method of estimating solutions with rain is to assume θ is precisely constant in the rainband, and to use (2.37) to represent forcing by latent heating. We defer details of this approach to section 7, where it is applied to zonally-varying cases.

Calculations have also been made for the quartic profile

$$\theta_s = 1 - (y/b)^4 \qquad (5.14)$$

by solving (5.1) numerically. Analytic estimates can also be made: (4.5) with this θ_s has a particular solution with v proportional to y. Results for $b = 4$, $\hat{q} = 8/9$, $\varepsilon = 0.1$ can be seen in Fig. 12. The very flat shape of this θ_s around the equator leads to a much wider rainband than for parabolic θ_s. Upward motion is weak, however, and net precipitation is nearly half that obtained in the parabolic case. Precipitation location and amount for a range of $\hat{q}$ for the quartic case are included in Fig. 10 for comparison. Rainband width decreases very slowly as $\hat{q}$ increases, until $\hat{q}$ is very close to unity.

6. ZONALLY VARYING STEADY SOLUTIONS WITH NO LATENT HEATING

In the absence of latent heating the model is linear, so zonally varying and zonally symmetric components can be determined separately. For small friction we show in this section that the dynamics of the zonal variations is quite different from that of the zonal average.

A zonal average will be denoted by an overbar, and departures are indicated by '; thus

$$v(x,y) = \bar{v}(y) + v'(x,y) \quad .$$

From equ. (2.30) for v we find that $\bar{v}$ and v' are both $O(\varepsilon)$ when θ_s is O(1). If terms $O(\varepsilon^2)$ are neglected then (2.30) gives

$$\beta v'_x = \varepsilon f \theta_s'_x \tag{6.1a}$$

which on integrating with respect to x becomes

$$\beta v' = \varepsilon f \theta_s' \quad . \tag{6.1b}$$

(Remember that $\beta = 1/2$ and $f = y/2$.) Similarly, equ. (2.31) leads to

$$\begin{aligned} u'_x &= -v'_y - \varepsilon \theta_s' \\ &= -2\varepsilon (f \theta_s'_y + \theta_s') \end{aligned} \tag{6.2}$$

Thus u' is $O(\varepsilon)$, in contrast to $\bar{u}$ which is O(1) as found in section 4. Eq. (2.32) likewise gives

$$\theta'_x = -fv'$$
$$= -2\varepsilon f^2 \theta_s' \quad , \qquad (6.3)$$

so θ' is also $O(\varepsilon)$, again contrasting with $\bar{\theta}$ which is $O(1)$. Further, θ' vanishes on the equator according to (6.3), so very little zonal variation in potential temperature is expected near the equator.

From the temperature equation (2.26) we deduce to $O(\varepsilon)$ that

$$w' = \varepsilon \theta_s' \quad . \qquad (6.4)$$

Consistently, the Sverdrup relation

$$\beta v' = fw' \qquad (6.5)$$

is a good approximation for the zonally-varying flow.

The approximations (6.1)-(6.5) could alternatively have been derived by neglecting Rayleigh friction and Newtonian cooling in the basic equations (2.24)-(2.26). In this limit (studied by Gill and Phlips 1986) v' and w' are in phase with the forcing θ_s', whereas u' and θ' are out of phase with θ_s'.

. Phases are such that upward motion is fed by zonal low-level inflow, as in a Walker cell.

This "no friction/no cooling" limit can be compared with the "large friction" limit in which frictional and cooling terms dominate zonal variations when ε >> zonal wavenumber. In this "large-friction" limit each longitude behaves independently, and

equations for v' etc. take the same form as those for $\bar{v}$ etc. in section 4. Then θ' is O(1), and in phase with θ_s'. Upward motion is now balanced by meridional convergence, as in a Hadley cell.

For the forcing used in section 3, zonal variations have wavenumber $k = \pi/8$ which is larger than the largest value of ε considered here, namely 0.1, so the "no friction/no cooling" limit should be a reasonable approximation. However, we find that a better approximation is to neglect Rayleigh friction but not the Newtonian cooling. Then the approximate form of (2.30) is

$$\beta v_x' - \varepsilon f^2 v' = \varepsilon f \theta_{sx}' \qquad (6.6)$$

Near the equator there is little difference from (6.1a), but the factor f^2 makes the Newtonian cooling increasingly important away from the equator. (Rayleigh friction terms are not affected in this way, so their omission is consistent.) This use of exactly geostrophic momentum balance while retaining thermal decay has an oceanic counterpart in equations for the thermocline, wherein friction is neglected but diffusion retained.

For this "frictionless" model eqns. (6.1b)-(6.4) are modified to

$$\beta v' = \varepsilon f(\theta_s' - \theta') \qquad (6.7)$$

$$u_x' = -2\varepsilon[f(\theta_s' - \theta')_y + \theta_s' - \theta'] \qquad (6.8)$$

$$\theta_x' = -2\varepsilon f^2(\theta_s' - \theta') \qquad (6.9)$$

$$w' = \varepsilon (\theta_s' - \theta') \quad . \tag{6.10}$$

The Sverdrup balance (6.5) still applies. These equations can easily be solved latitude-by-latitude, given θ_s'.

To illustrate the various approximations we use the Pacific forcing (3.1) for January. Amplitude and phase lag (relative to θ_s') of u', v', w', and θ' are shown in Fig. 13 for the "frictionless" and "no friction/no cooling" estimates, along with the exact solution found by numerical methods. The forcing has the same phase at all latitudes, and its meridional profile is the same as that of w' for the "no friction/no cooling" limit. For the "frictionless" case, the phase lag is $\pm \arctan(\varepsilon f^2/\beta k)$ for v', θ' and w', independent of the amplitude of the forcing θ_s'.

Generally, amplitudes obtained from the "frictionless" model are larger than for the exact calculation, and "no friction/no cooling" amplitudes are larger still, while meridional structure is broadly the same in each case. The "frictionless" model estimates phase lags much better than the "no friction no cooling" model. The approximations are poorest for the phase lags of θ' and v' near the equator; however these quantities also have low amplitude there so the error is not significant. Phases are such that there is low-level zonal flow into and meridional flow away from a maximum of θ_s' near the equator, where there is upward motion.

7. ZONALLY VARYING STEADY SOLUTIONS: MOIST CASE

As in section 5, some insight into the dynamics of the zonally-varying model with rain can be obtained by considering the limit $\hat{q} \to 1$, because the precipitation region then shrinks to a small area around the position (x_0, y_0) of the maximum value θ_{s0} of the forcing θ_s. The method of matching approximate solutions in the areas with and without precipitation used for the zonally symmetric case is difficult to apply when the unknown boundary varies in two dimensions, so we describe here another method in which θ is assumed constant (θ_c say) where there is precipitation. The results in section 3 show that this approximation is reasonable; more rigorous analysis is difficult.

With this assumption, the forcing temperature θ_L associated with latent heating becomes, from (2.37),

$$\theta_L = P/E = \begin{cases} (\theta_s - \theta_L)\,\hat{q}/(1-\hat{q}) & \text{precipitation} \\ 0 & \text{no precipitation} \end{cases} \qquad (7.1)$$

and the boundary of the wet region is the contour of θ_s with $\theta_s = \theta_c$. The response to θ_s and θ_L can be determined separately using the linear dry equations and superimposed, as described in section 2. Then θ_c can be determined by requiring

$$\theta_c = \theta_0 \text{ (due to } \theta_s) + \theta_0 \text{ (due to } \theta_L) \qquad (7.2)$$

where the subscript $_o$ denotes values at the point x_o, y_o .

It is useful to further split θ_L into the zonal average

$$\bar{\theta}_L = \frac{1}{\ell} \int_0^{\ell} \theta_L \, dx$$

(where ℓ is the length of the periodic channel), and the departure θ_L'. The response to these components can be calculated separately, as in sections 4 and 6, and superimposed. This procedure is also informative because the total precipitation P_{TOT} is determined solely by $\bar{\theta}_L$, as follows:

$$P_{TOT} = \iint P \, dxdy \qquad (7.3a)$$

$$= \varepsilon \ell I$$

where

$$I = \int_{y_-}^{y_+} \bar{\theta}_L \, dy \qquad (7.3b)$$

with y_- and y_+ being the southern and northern extremities of the precipitation region.

When the width $y_+ - y_-$ is small, the response to $\bar{\theta}_L$ can be estimated by using

$$\bar{\theta}_L \approx I \, \delta(y-y_o) \qquad (7.4)$$

Then $\bar{v}$ and $\bar{\theta}$ due to $\bar{\theta}_L$ are given by expressions (4.12) and (4.13) multiplied by the strength factor I. In particular, (4.13) gives

$$\bar{\theta}_o \text{ (due to } \bar{\theta}_L) = -I \, H_y(-y_o) \, H_y(y_o) \, / \, W \, . \qquad (7.5)$$

The zonally-varying component θ' is small when ε is small, as shown in section 6. If the response to θ_s' and θ_c' is neglected, then the matching condition (7.2) can be written

$$r^2 = [\theta_{s_0} - \bar{\theta}_0(\text{due to } \bar{\theta}_s)] - \bar{\theta}_0(\text{due to } \bar{\theta}_c) \qquad (7.6)$$

where we have defined

$$r^2 = \theta_{s_0} - \theta_c \quad . \qquad (7.7)$$

Note that r is a measure of the length scale of the wet region (more details are given below). For a roughly circular patch of rain, I is $O[r^4 \hat{q}/(1-\hat{q})]$. The term [ ] in (7.6) is O(1), so for small r (and $\hat{q}$ close to unity) solution of (7.6) requires

$$r \sim (1-\hat{q})^{1/4} \quad . \qquad (7.8)$$

The left-hand-side of (7.6) is then negligible, and equating the terms on the right-hand-side gives an expression for I. (Equivalently, the first estimate for θ_c is $\theta_c = \theta_{s_0}$.) Hence we obtain an estimate of the total precipitation as

$$P_{TOT} = \frac{\varepsilon \ell W}{-H_y(-y_0)H_y(y_0)} \{\theta_{s_0} - \bar{\theta}_0(\text{due to } \bar{\theta}_s)\} \qquad (7.9)$$

The term { } is obtained from the dry zonally-symmetric model. Note that this estimate of P_{TOT} is independent of $\hat{q}$.

The position of the wet region can next be improved by solving

$$\tfrac{1}{2}\,\varepsilon \iint \theta_s - \theta_c + |\theta_s - \theta_c|\, dxdy = P_{TOT}\,(1-\hat{q})/\hat{q} \qquad (7.10)$$

to determine θ_c, which can easily be done numerically. (The form of the integrand ensures that only values from the region of precipitation contribute, where $\theta_s > \theta_c$.)

If the area of rain is a zonal strip rather than a circular patch, then I turns out to be $O[r^3 \hat{q}/(1-\hat{q})]$, and for small r we regain the zonally-symmetric result of section 5, namely that the width of the strip is $O[(1-\hat{q})^{1/3}]$. The precipitation estimate (7.9) is unchanged.

To be more specific regarding this calculation of precipitation position, suppose that near (x_0, y_0) the forcing takes the quadratic form

$$\theta_s = \theta_{s0} - A^2(x-x_0)^2 - B^2(y-y_0)^2 \qquad (7.11)$$

Then the approximate region of rain is elliptical, within which

$$\theta_L = [\, r^2 - A^2(x-x_0)^2 - B^2(y-y_0)^2 \,]\, \hat{q}/(1-\hat{q}) \qquad (7.12)$$

with r^2 given by (7.7). (The length scale is now clearly O(r).) This leads to

$$\bar{\theta}_L = \begin{cases} \dfrac{4}{3\ell}\,\dfrac{\hat{q}}{1-\hat{q}}\,\dfrac{1}{A}\,[r^2 - B^2(y-y_0)^2]^{3/2} & y_- < y < y_+ \\ 0 & \text{otherwise} \end{cases} \qquad (7.13)$$

with $y_+ = y_o + r/B$ and $y_- = y_o - r/B$. (Here we have assumed that the ellipse closes within the periodic channel. Modifications if A = 0, for example, can be easily made.) Hence in this case (7.10) gives

$$P_{TOT} = \varepsilon \frac{\pi}{2} \frac{\hat{q}}{1-\hat{q}} \frac{r^4}{AB} \tag{7.14}$$

and an expression for r follows from equating (7.14) with (7.9). The area of rain is

$$\pi r^2 / AB \ . \tag{7.15}$$

As a particular example we consider January Pacific forcing which, as defined in section 3, has a maximum value $\Theta_{s_0} = 1$ at $x_o = -4$, $y_o = 0$. (i.e. at the equator in the western Pacific). Near this point the shape (7.12) requires A = 0.12, B = 0.25, and using (7.5) and (7.14) gives

$$\bar{\Theta}_o(\text{due to } \bar{\Theta}_L) = 0.8 \ r^4 \ \hat{q}/(1-\hat{q}) \ . \tag{7.16}$$

The dry response to Θ_s is

$$\bar{\Theta}_o \ (\text{due to } \bar{\Theta}_s) = 0.7$$

[$\Theta_o'(\text{due to } \Theta_s') = 0.02$, which is negligible.]

Hence we obtain the estimates

$$P_{TOT} = 20 \ \varepsilon \tag{7.17a}$$

$$r = 0.8\,[(1-\hat{q})/\hat{q}]^{1/4}, \qquad (7.17b)$$

$$\text{area} = 65\,[(1-\hat{q})/\hat{q}]^{1/2} \qquad (7.17c)$$

For various $\hat{q}$, and $\varepsilon = 0.1$, these estimates are shown in Fig. 14 along with numerical results obtained by integrating the time-dependent equations to equilibrium. (The numerical results may differ significantly from exact solutions when $\hat{q} > .99$ due to difficulties in resolving the small regions of rain.) The precipitation estimate (7.17a) is about double the numerical results, and should be regarded as an upper bound. The area estimate (7.17c) seems to be a surprisingly good approximation, showing the correct trend as $\hat{q}$ varies, with slightly small magnitude.

Revised estimates were also made by solving the dry equations with forcing $\bar{\theta}_e$ of the form (7.13) in place of the δ - function (7.4), i.e. allowing finite width of the precipitation region, and the results are included in Fig. 14. Precipitation amount is improved, but the area is further reduced, so the area estimate (7.17c) must be regarded as fortuitously good.

8. THE EFFECT OF VARYING THE ZONAL FORCING GRADIENT

When forcing is zonally symmetric then there is a zonal band of precipitation fed by meridional low-level inflow, as in Hadley circulation. In this section we examine the effect of increasing the zonal variation in the forcing θ_s, to see at what point the zonal band of precipitation breaks and Walker-type circulation becomes evident.

Forcing of the form

$$\theta_s = \theta_w(y) \; [\, 1 - \gamma \sin (\pi x/8)] \qquad (8.1)$$

is used, with θ_w as defined in (3.2) for the West Pacific, for January (maximum on the equator) and July (maximum north of the equator). This choice is not meant to represent any actual physical situation, but merely to provide convenient examples. The parameter γ controls the zonal contrast in θ_s.

In each case the time-dependent equations were integrated to a near-steady state at time $t = 60$ (as in section 3), using $\varepsilon = 0.1$, $\nu = 0$, $\hat{q} = 8/9$.

This section ends with a brief description of a related seasonal cycle experiment.

8.1. MAXIMUM FORCING ON EQUATOR

With γ increasing from zero in steps of 0.01, the precipitation pattern switches from a continuous band to an elongated patch on

reaching γ = 0.06. Changes in the pattern up to this point and beyond are gradual: the rainband thins and breaks near x = 4, where θ_s is weakest along the equator, and broadens near x = -4 where θ_s is strongest. Total precipitation increases slightly over a diminishing area as increases: P_{TOT} = 0.68 over area = 32 for γ = 0, while P_{TOT} = 0.76 over area = 19 for γ = 0.1 .

The forcing θ_s for γ = 0.06 can be seen in Fig. 15, together with low-level wind components and the precipitation map. The mid-level vertical velocity pattern (not shown) is almost identical to the precipitation — low-level divergence at the equator first appears where and when the rainband breaks. Meridional low-level flow is everywhere equatorward, so any equatorial divergence must be associated with the zonal flow. Fig. 15b shows equatorial westerlies within the precipitation region and easterlies elsewhere, reflecting a balance of frictional and pressure gradient terms along the equator. The zonal flow also contributes significantly to the convergence in the precipitation region. The temperature field (not shown) looks like the forcing pattern in Fig. 15a, but with markedly less zonal contrast.

Evidently only a weak zonal contrast in θ_s is sufficient to generate a Walker-like circulation.

8.2 MAXIMUM FORCING OFF EQUATOR

In this case θ_s is largest at y = 1.5, about 15°N. When γ is again increased in steps of 0.01 there is a gradual change in the precipitation pattern, with the zonal band breaking at γ = 0.20.

There is little change in total precipitation, but the area decreases markedly: P_{TOT} = 1.3 over area = 32 for γ = 0, and P_{TOT} = 1.4 over area 19 for γ = 0.3 .

Maps of θ_s, u, v and P for γ = 0.20 are shown in Fig. 16. As before, the rainband breaks near x = 4 where is relatively low. The map of meridional velocity shows quite strong cross-equatorial flow directed northward into and across the region of precipitation, with weaker southward flow to the north-west of the precipitation. This component again is weakly convergent at the break in the rainband.

The zonal flow is westerly in a strip north of the equator, with maximum strength just to the west of the heaviest precipitation and minimum west of the break in the rainband. The zonal gradient is sufficient to provide the low-level divergence required at the break, and to boost convergence across the centre of the precipitation region. Just west of the break there is a "doldrums" region of very light winds.

Compared to the previous case we see that considerably larger zonal contrast in θ_s is required to break the rainband off the equator. Due to Coriolis effects the zonal temperature gradient is less efficient at driving a zonal wind gradient away from the equator.

8.3 A seasonal cycle experiment

A simple seasonal cycle experiment was carried out by prescribing

$$\theta_s = \tfrac{1}{2}\theta_{JAN}[\,1+\cos(\omega t)\,] + \tfrac{1}{2}\theta_{JUL}[\,1-\cos(\omega t)\,] \quad (8.2)$$

where θ_{JAN} and θ_{JUL} are the January and July forcing fields described in section 3, and

$$\omega = 2\pi / 1440 \qquad (8.3)$$

corresponds to a dimensional period of about 360 days. The maximum zonal forcing gradient changes in amplitude and location with time, being largest and closest to the equator in the model January when t=0. The changes are slow compared to the atmospheric equilibration time of about 15 days (for $\varepsilon = 0.1$), and the response is found to be almost in equilibrium with θ_s at all times following an initial spin-up period. Accordingly the precipitation pattern gradually changes between those shown in Fig. 6 for January and July.

The equatorial zonal forcing contrast in January is 0.33, which is much larger than that found to break the rainband in section 8.1, so there is then a patch of precipitation located over the maximum in θ_s, with accompanying Walker-type circulation. Likewise, the July forcing zonal contrast of 0.13 north of the equator is too weak to break the rainband and a zonal precipitation pattern appears. Intermediate patterns for March and May can be seen in Fig. 17: after January the precipitation zone shifts north of the equator, developing a north-eastward extension which then elongates to form a zonal strip. The sequence reverses from July to January.

9. Summary

A simple model with dynamic moisture effects has been used to examine the response of the tropical atmosphere to various simple heating distributions. Forcing related to sea-surface temperature is prescribed, but precipitation is determined by the interaction of the atmospheric circulation and the moisture field, so the model selects its own latent heat release pattern. In the steady model, precipitation always occurs at the location of the maximum prescribed heating: at such a point low-level flow is convergent and moisture levels are soon driven to saturation both by evaporation and by low-level advection. The consequent latent heat release then adds to the prescribed heating, initiating a 'convergence feedback' process. This process is limited by the influx of surrounding drier air and by friction and Newtonian cooling.

With forcing based on idealised Pacific SST, qualitatively correct precipitation patterns were obtained. In January, when SST is largest in the equatorial west Pacific, rainfall is concentrated in a patch overlying the SST maximum, whereas a continuous zonal band of rain appears in July when there is less zonal SST contrast and the maximum SST is north of the equator. For the January case circulation is Walker-like with zonal flow feeding the upward motion in the precipitation region, but in July the circulation is Hadley-like with meridional flow feeding the upward motion.

The zonally symmetric version of the model with and without latent heating is sufficiently simple to allow analytic solution of some special cases. In particular, the effect of the saturation

moisture level $\hat{q}$ on the amount and extent of precipitation was analysed. The area of rainfall is closely proportional to $(1-\hat{q})^{1/3}$, so as $\hat{q}$ approaches the critical value of 1 from below (so latent heating increasingly cancels adiabatic cooling) the precipitation band shrinks toward a point above the SST maximum, while upward motion increases correspondingly. (The limit is not reached in practise, as diffusive and nonlinear effects become important on small scales.)

When zonal variations are included the problem is complicated by the two-dimensional boundary of the precipitation region, which must be determined. We estimate that the rainfall area is proportional to $(1-\hat{q})^{1/2}$ for an elliptical pattern, and net precipitation is weakly dependent on $\hat{q}$, in general agreement with numerical results. Whether the precipitation pattern is zonal or a patch depends on the size and position of the maximum zonal forcing variation. On the equator weak variation is sufficient to drive a Walker circulation, whereas stronger variation is required to break a zonal rainband further from the equator.

With such a simple model one can think of a long list of alterations to improve the agreement with observations and to add to the physics. One aspect that was initially tested was to make $\hat{q}$ temperature dependent, as in Gill (1982b). This had only a small quantitative effect so for simplicity $\hat{q}$ was subsequently taken to be constant. Another effect yet to be investigated is to allow evaporation to increase with windspeed.

The model wind is purely baroclinic: a fixed barotropic component

could be added, and one effect to be studied would be the flow required to shift precipitation away from the position of maximum prescribed heating. The simple vertical structure also means that a proper understanding of the relation between the prescribed heating and SST is beyond the scope of this model, but this is certainly needed. Further investigations using general circulation models of the atmosphere could be made.

The effects of land distribution have been omitted. Any model covering the entire tropics will need some representation of the continents: some preliminary calculations have been made by simply setting evaporation to zero over 'land'.

Quantitative aspects of the model need further study. For example, latent heating has the same magnitude as the prescribed heating in the model, but latent heating in the tropics is observed to be far more dominant.

Finally, to address the problem of tropical ocean-atmosphere interaction the underlying SST should respond in some way to the atmospheric winds. A correspondingly simple ocean model is being constructed for this purpose.

REFERENCES

Abramowitz, M. & I.A. Stegun (1970) Handbook of Mathematical Functions. Dover Publications, N.Y. 1046pp

Davey, M.K. (1985) Results from a moist equatorial atmosphere model. In: Coupled Ocean-Atmosphere Models (ed. J.C.J. Nihoul). Elsevier Oceanography Series 40, 41-49.

Gill, A.E. (1980) Some simple solutions for heat-induced tropical circulation. Q.J.Roy.Met.Soc. 106 447-462.

Gill, A.E. (1982a) Atmosphere-Ocean Dynamics. Academic Press, New York, N.Y. 662pp.

Gill, A.E. (1982b) Studies of moisture effects in simple atmospheric models: the stable case. Geophys.Astrophys.Fluid Dyn. 19, 119-152.

Gill, A.E. (1982c) Spontaneously growing hurricanelike disturbances in a simple baroclinic model with latent heat release. In: Topics in Atmospheric and Oceanic Sciences: Intense Atmospheric Vortices. (ed. Bengtsson/Lighthill) Springer Verlag. 111-129.

Gill, A.E. (1985) Elements of coupled ocean-atmosphere models for the tropics. In: Coupled Ocean-Atmosphere Models (ed. J.C.J. Nihoul) Elsevier Oceanography Series 40, 303-327.

Gill, A.E & P.J. Phlips (1986) Nonlinear effects on heat-induced circulations of the tropical atmosphere. Q.J.Roy.Met.Soc.

112,69-92.

Heckley, W.A. &
A.E. Gill (1984) Some simple analytic solutions to the problem of forced equatorial long waves. Q.J.Roy.Met.Soc. 110,203-217.

Held, I.M. &
M.J. Suarez (1978) A two-level primitive equation atmospheric model designed for climatic sensitivity experiments. J.Atmos.Sci. 35,206-229

Lau, K.M. &
H. Lim (1982) Thermally driven motions in an equatorial beta-plane: Hadley and Walker circulations during the winter monsoon. Mon. Weath. Rev. 110, 336-353.

Lim, H. &
C-P. Chang (1983) Dynamics of teleconnections and Walker circulations forced by equatorial heating. J.Atmos.Sci. 40, 1897-1915.

Lorenz, E.N. (1984) Formulation of a low order model of a moist general circulation. J.Atmos.Sci. 41, 1933-1945

Phlips, P.J. &
A.E. Gill (1986) An analytic model of the heat-induced tropical circulation in the presence of a mean wind. Submitted to Q.J.Roy.Met.Soc.

Rowntree, P.R. (1976) The influence of tropical east Pacific Ocean temperatures on the atmosphere. Q.J.Roy.Met.Soc. 98, 290-321.

Webster, P.J. (1972) Response to the tropical atmosphere to local steady forcing. Mon.Weath. Rev. 100, 518-541.

Webster, P.J. (1981) Mechanisms determining the atmospheric response to sea surface temperature anomalies. J.Atmos. Sci. 38, 554-571.

Zebiak, S.E. (1982) A simple atmospheric model of relevance to El Nino. J.Atmos.Sci. 39, 2017-2027.

FIGURE CAPTIONS

Fig. 1 Vertical structure assumed in the model. Potential temperature perturbation θ^* and vertical velocity w^* are largest at the mid-troposphere level. Horizontal velocity $\underset{\sim}{u}^*$ has largest and opposite values at lower and upper levels. Specific humidity s^* is concentrated at low levels.

Fig. 2 Forcing temperature θ_s has a pattern representing tropical Pacific sea-surface temperatures. (a) January (b) July Zonal and meridional cross-sections indicated by arrows are shown below and to the right of the contour maps. Distance units are equatorial Rossby radii, about 10^c of latitude or longitude. The mid-level heating rate is $\varepsilon\theta_s$.

Fig. 3 Mid-level potential temperature perturbation θ at time t=60 (about 15 days), effectively a steady state, for the model with $\varepsilon = 0.1$, $\nu = 0.025$, $\hat{q} = 8/9$ (a) January (b) July

Fig. 4 Low-level wind (u,v) at time t=60, for $\varepsilon = 0.1$, $\nu = 0.025$, $\hat{q} = 8/9$. Upper-level wind is oppositely directed. (a) January (b) July

Fig. 5 Dryness $1-q/\hat{q}$ at time t=60, for $\varepsilon = 0.1$, $\nu = 0.025$, $\hat{q} = 8/9$. Within the dotted zero contour $q=\hat{q}$ and precipitation

will occur where there is low-level convergence. (a) January (b) July

Fig. 6 Precipitation P at time t=60 for $\varepsilon = 0.1$, $\nu = 0.025$, $\hat{q} = 8/9$. Non-dimensionally P is equal to the latent heating rate Q. The zero contour is dotted. (a) January (b) July

Fig. 7 The analytic response to the forcing temperature $\theta_s = 1-(y/4)^2$ for the steady zonally-symmetric model with no latent heating. (a) Meridional profiles of θ_s, mid-level potential temperature perturbation θ and vertical velocity w/ε, and low-level velocity components u and v/ε. (b) y-z plane showing the zonal flow u^* (south of the equator) and streamlines for the meridional flow (v^*, w^*) north of the equator. These patterns are symmetric about the equator.

Fig. 8 The analytic response to the forcing temperature $\theta_s = \delta(y-y_0)$ concentrated along the line $y=y_0$, for the steady zonally-symmetric model with no latent heating. Meridional profiles of mid-level potential temperature perturbation θ and low-level velocity components u and v/ε are shown for $y_0=0$ (solid) and $y_0=1$ (dashed). Vertical velocity w is related to θ by $w/\varepsilon = -\theta$ for $y \neq y_0$: balance of upward and downward motion is provided by a spike in w at y_0.

Fig. 9 Meridional low-level velocity v+ at the northern edge y+ of

the precipitation region, for the zonally-symmetric forcing $\theta_s = 1-(y/4)^2$. This analytic curve is given by eq. (5.8).

Fig. 10 Total precipitation P_{TOT} per unit zonal distance, and the width $y_+ - y_-$ of the precipitation region, in response to the zonally-symmetric forcing $\theta_s = 1-(y/4)^2$, for various values of $\hat{q}$. The dashed line is the precipitation estimate using a point source of latent heating, and the solid lines are estimates obtained allowing finite width. Solid circles correspond to numerical solutions of the exact equations. Open circles show numerical solutions with $\theta_s = 1-(y/4)^4$.

Fig. 11 The response to the forcing temperature $\theta_s = 1-(y/4)^2$ for the steady zonally-symmetric model with latent heating, for $\varepsilon = 0.1$, $\hat{q} = 8/9$. Meridional profiles of θ_s, mid-level potential temperature perturbation Θ and vertical velocity w/ε, and low-level horizontal velocity components u and v/ε are shown. Precipitation $P = \hat{q}w$ occurs where $w>0$.

Fig. 12, As Fig. 11, but for $\theta_s = 1-(y/4)^4$

Fig. 13 The zonally-varying components of the steady response to the 'January Pacific' forcing shown in (Fig. 2a), with no latent heating. Results are shown for analytic no-friction/no-cooling and no-friction models, together with numerical results with friction and cooling.

(a) Amplitude and phase of the mid-level vertical

velocity w'/ε . This is equal to θ_s' for the no-friction/no-cooling case.

(b) Amplitude and phase of the mid-level temperature perturbation θ'.

(c) Amplitude and phase of the zonal low-level velocity u'.

(d) Amplitude and phase of the meridional low-level velocity v'.

Fig. 14 Total precipitation P_{TOT} and area of precipitation for models with $\varepsilon = 0.1$ and various $\hat{q}$. Solid lines are for numerical results from time-dependent integrations. Long-dash lines show estimates obtained using a precipitation zone of infinitely-small width, and short-dash lines are for estimates obtained using a precipitation zone of finite width.

Fig. 15 The response to the forcing $\theta_s = \theta_w(y)\ [1-\gamma \sin(\pi x/8)\ ]$ with $\theta_w = 1-(y/4)^2$ and $\gamma = 0.06$, using $\varepsilon = 0.1$, $\hat{q} = 8/9$ (a) The forcing temperature θ_s. (b) The low-level zonal velocity u at time t=60 (effectively steady). The zero contour is dotted, and positive contours solid. (c) The low-level meridional velocity v at time t=60. (d) Precipitation P at time t=60.

Fig. 16 The response to forcing $\theta_s = \theta_w(y)\,[1-\gamma\sin(\pi x/8)]$ with $\theta_w = 1-(y-Y)^2(Y^2+2yY+16)/(Y^2+16)^2$, $Y = 1-5y$, and $\gamma = 0.2$ using $\varepsilon = 0.1$, $\hat{q} = 8/9$. (a) The forcing temperature (b) The low-level zonal velocity u at time t=60. (c) The meridional low-level velocity v at time t=60. (d) Precipitation P at time t=60.

Fig. 17 Precipitation patterns obtained using the seasonal-cycle forcing $\theta_s = \frac{1}{2}\theta_{JAN}\,[1+\cos(\pi\, t/720)] + \frac{1}{2}\theta_{JUL}\,[1-\cos(\pi\, t/720)]$ with $\varepsilon = 0.1$, $\hat{q} = 8/9$. (a) Time t=240 (March) (b) Time t=480 (May)

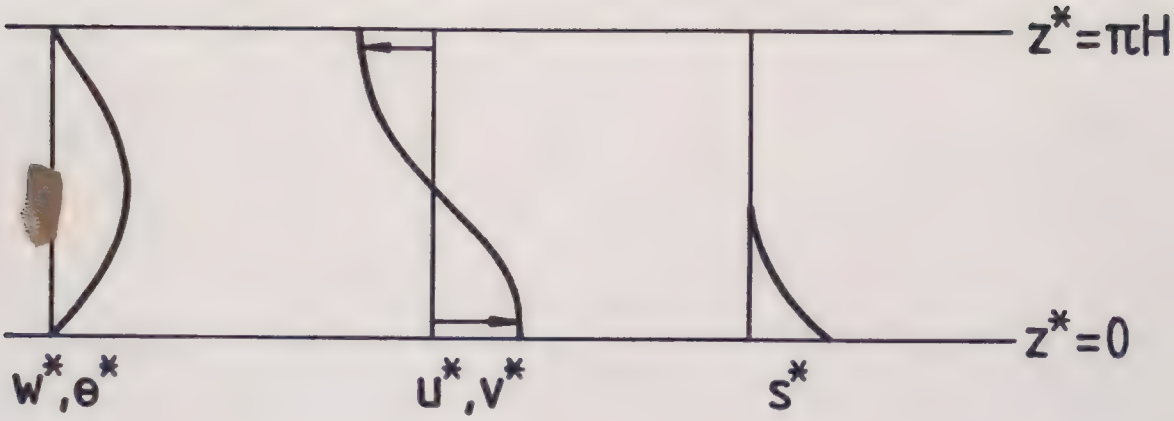

Fig. 1

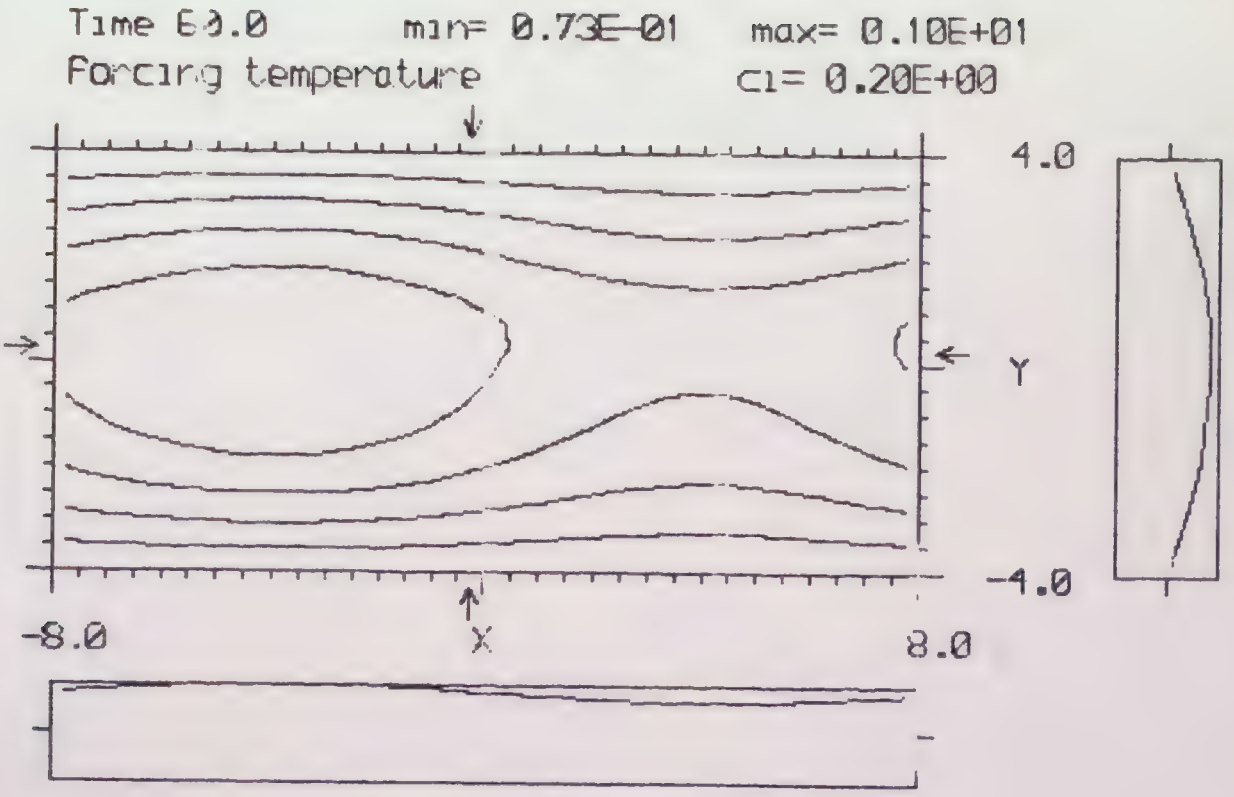

Fig. 2a (Jan)

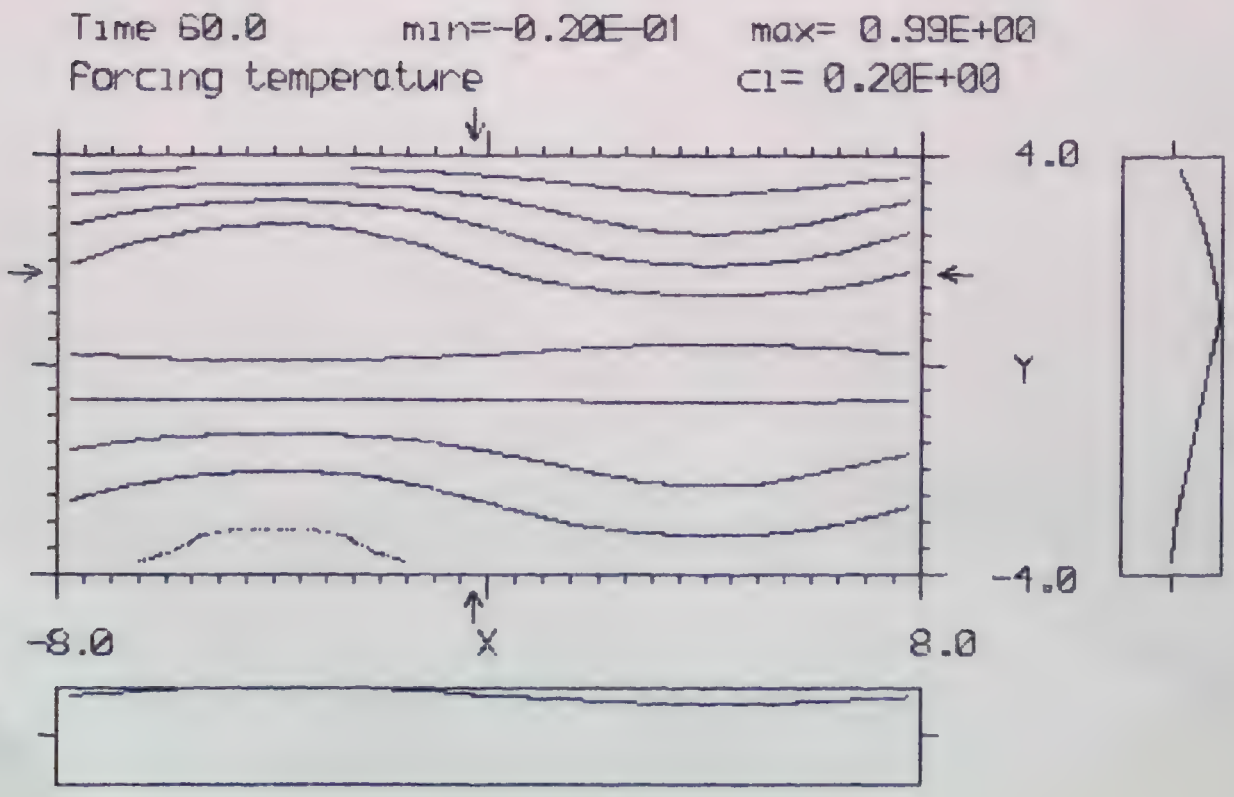

Fig 2b (July)

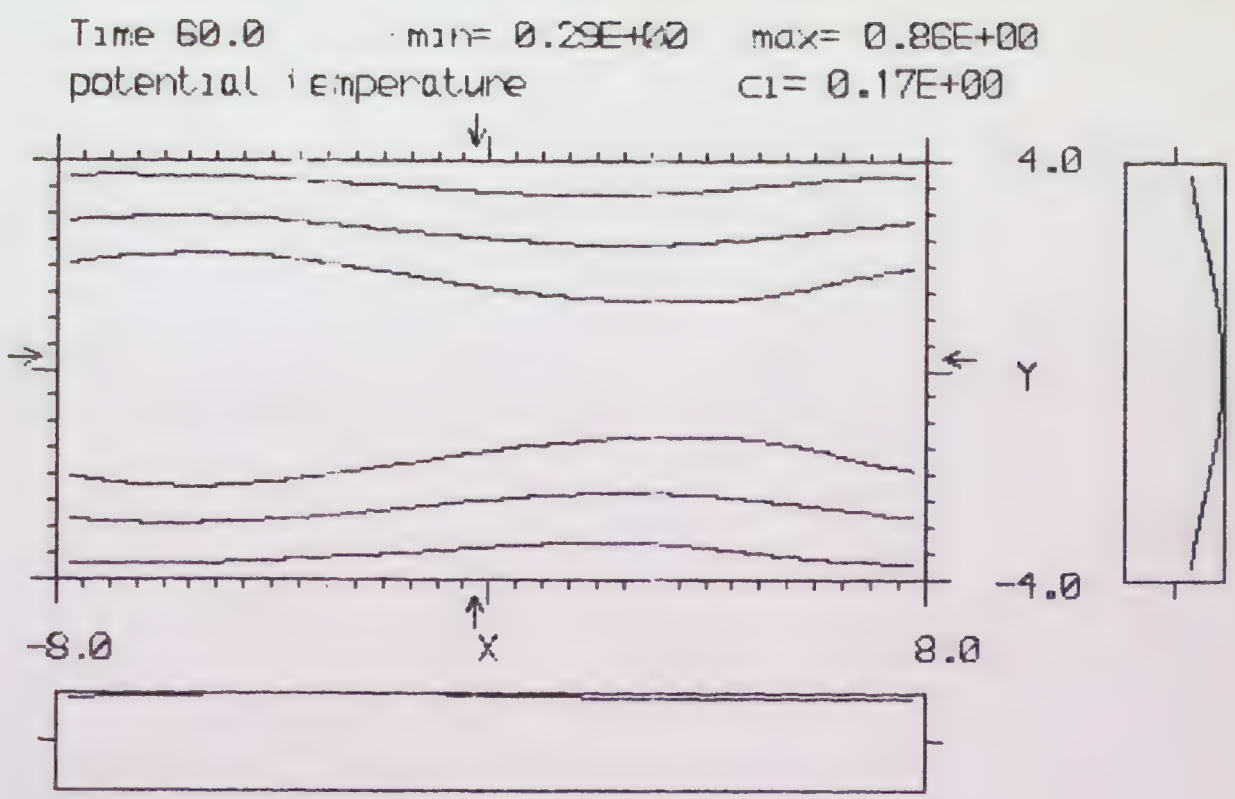

Fig. 3a (Jan)

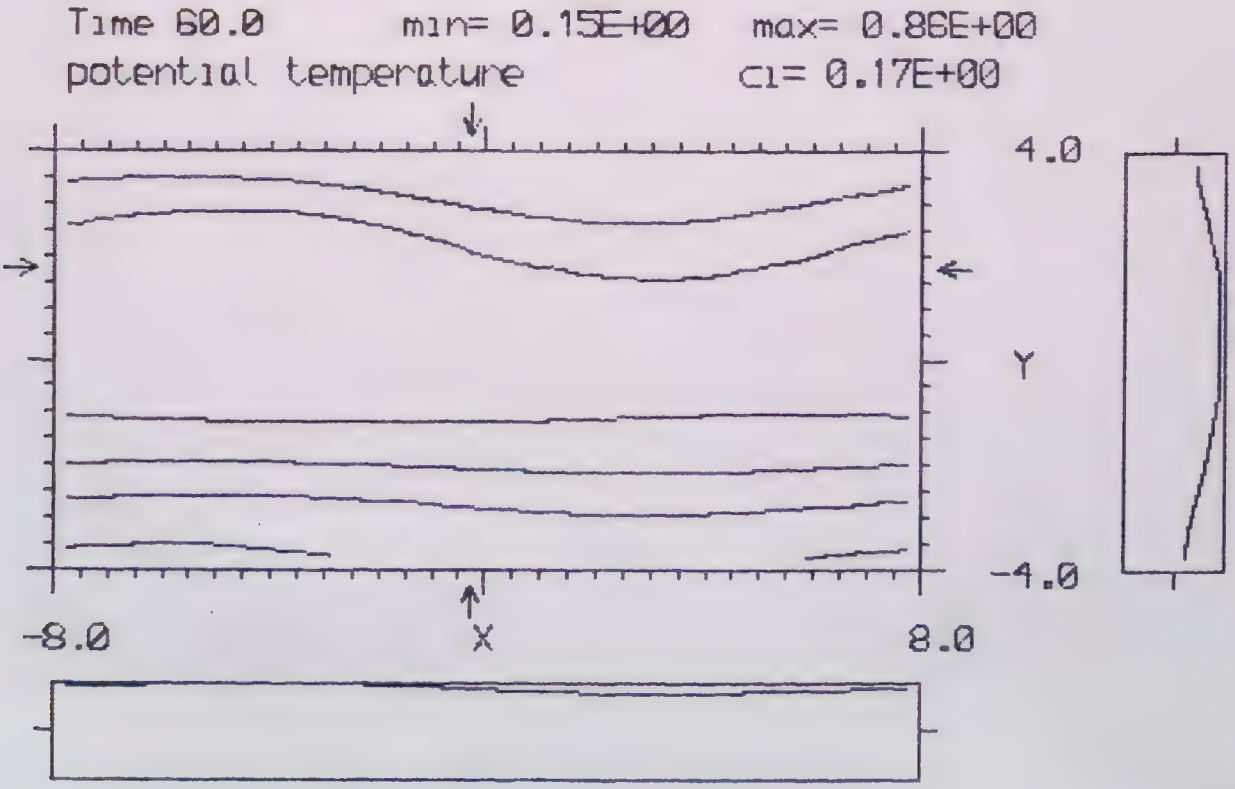

Fig. 3b (July)

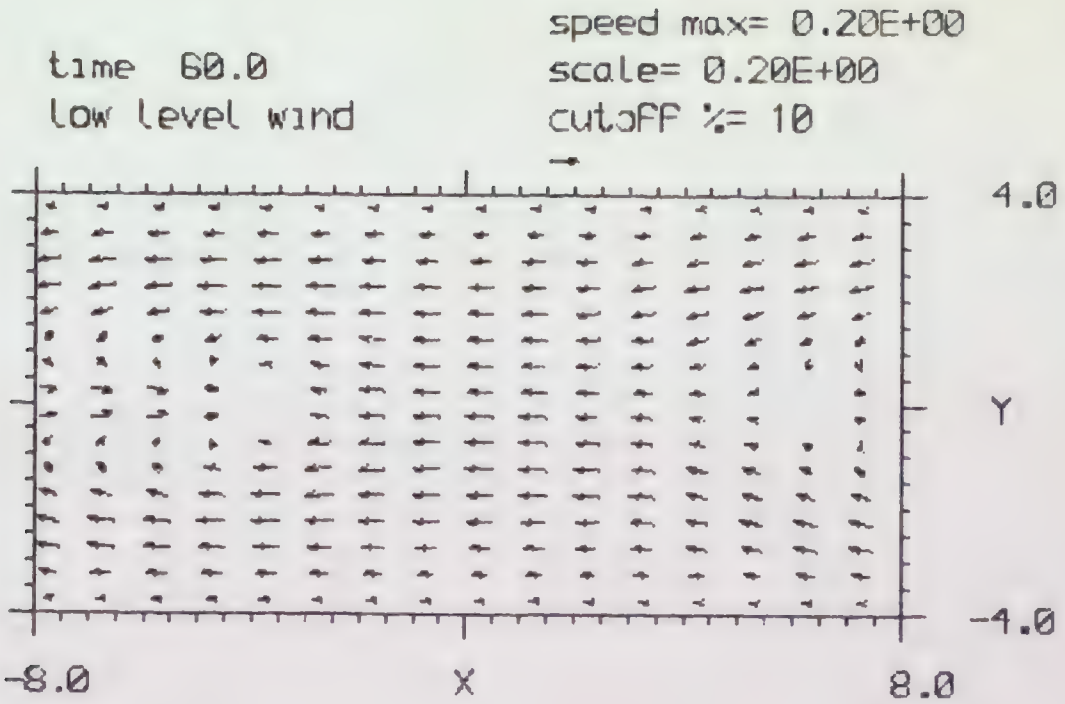

Fig. 4a (Jan)

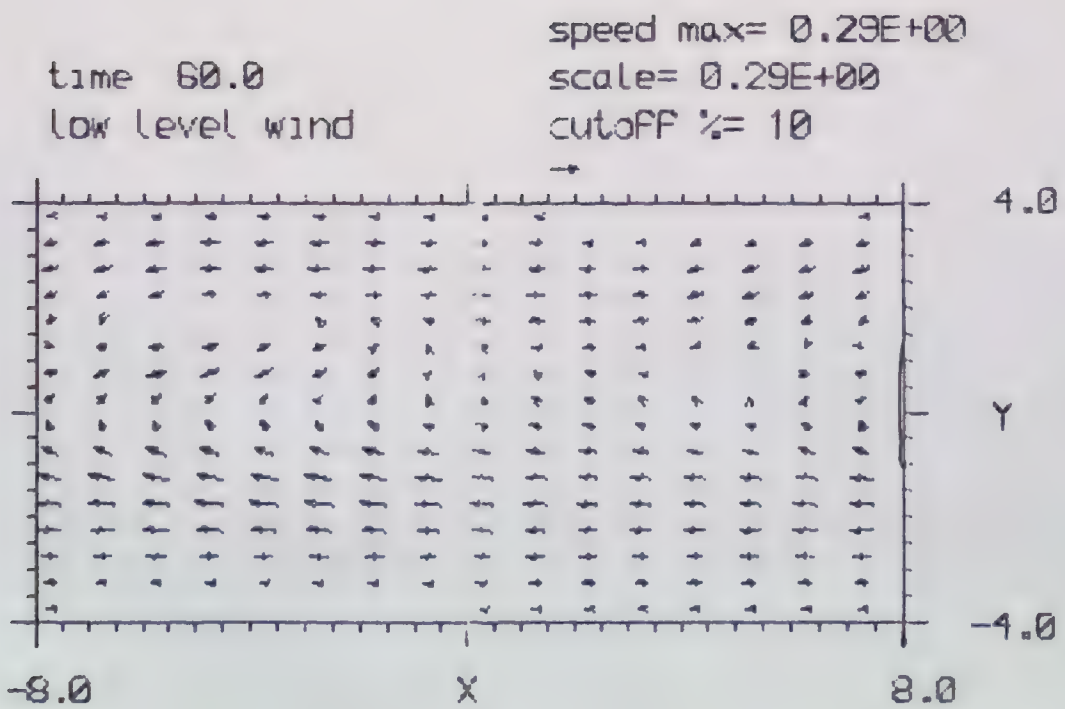

Fig. 4b (July)

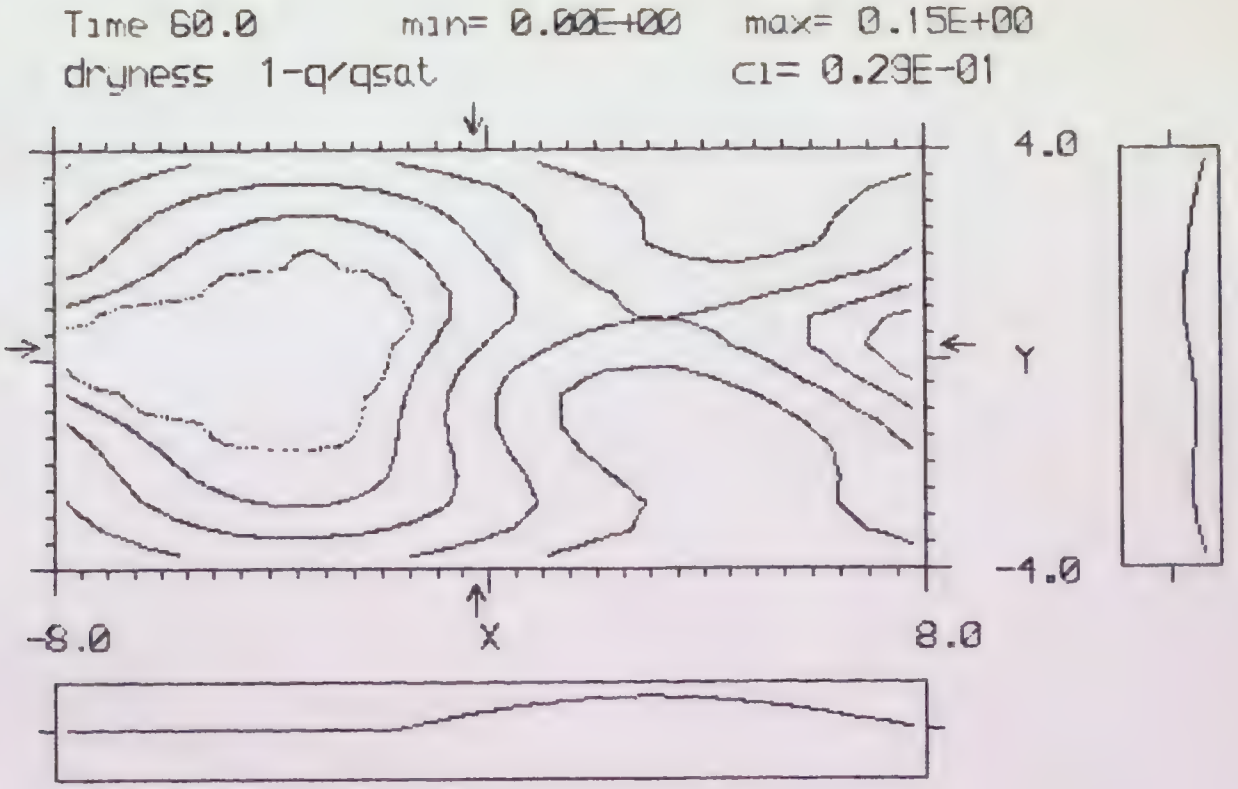

Fig. 5a (Jan.)

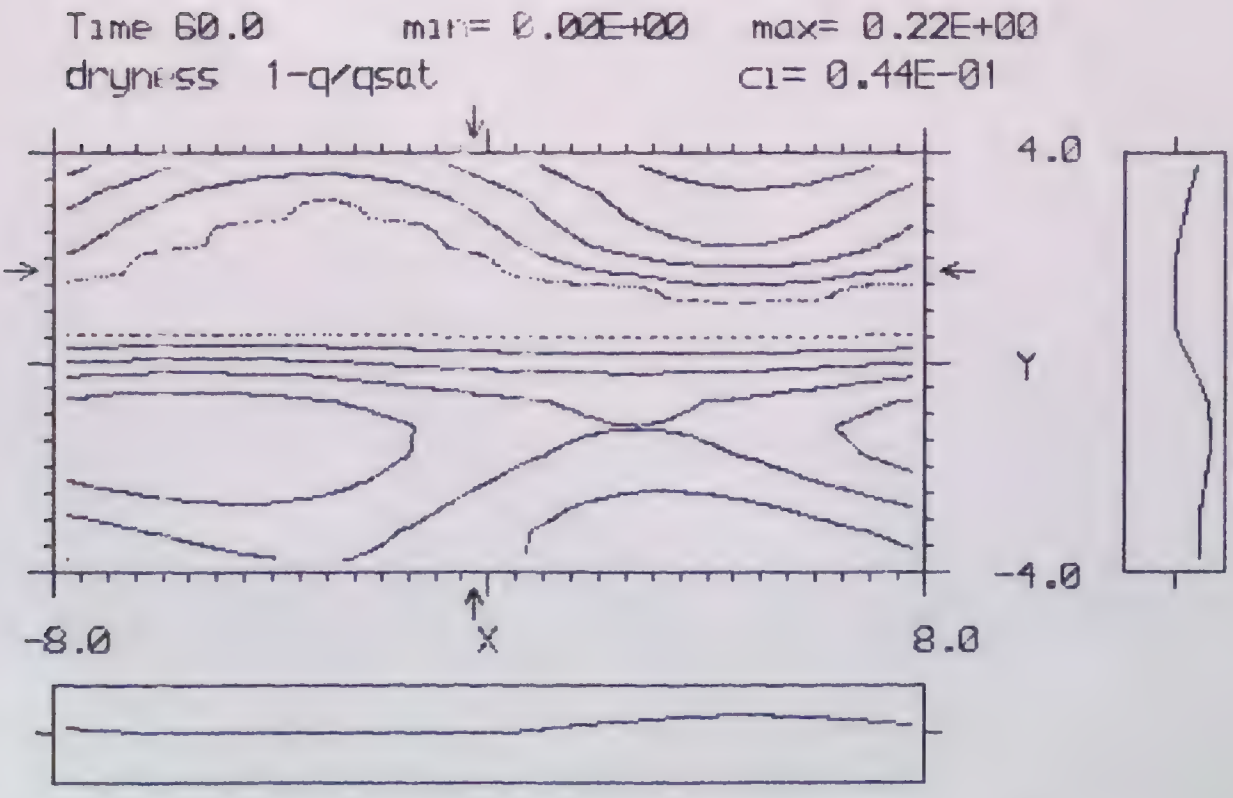

Fig. 5b (July)

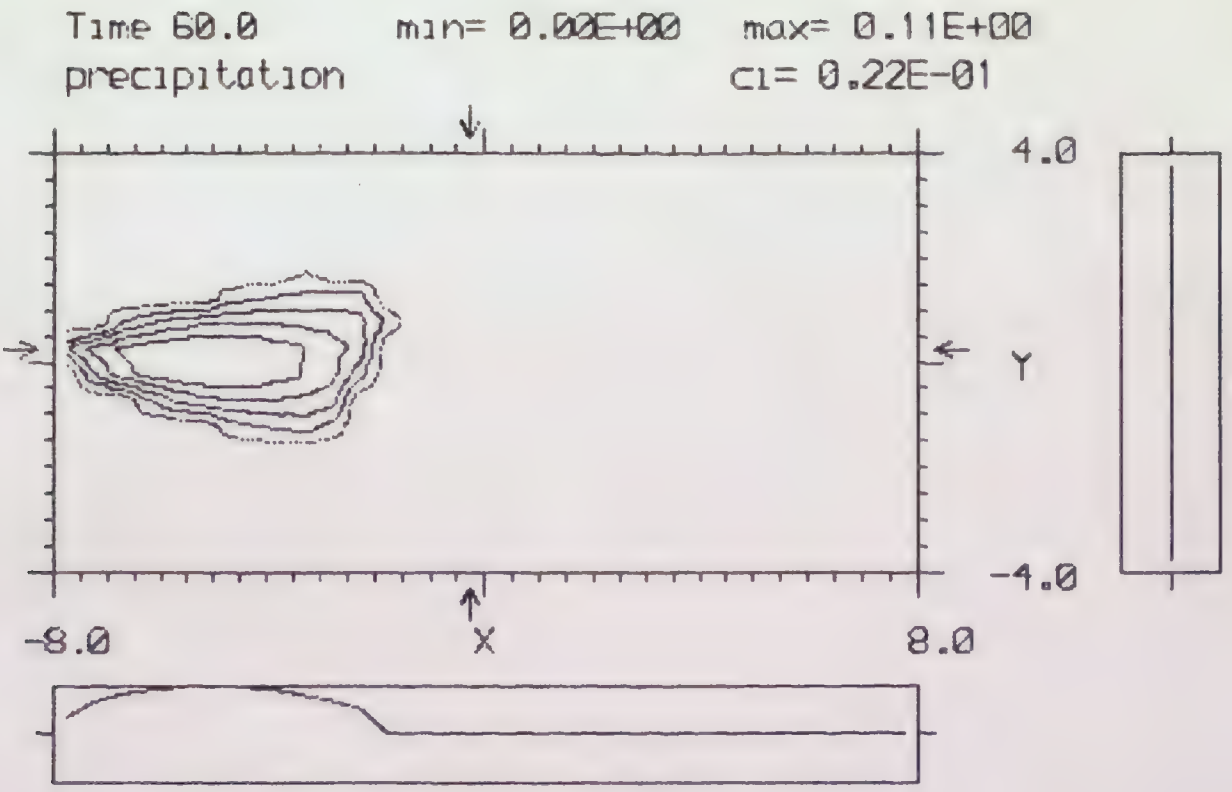

Fig. 6a (Jan.)

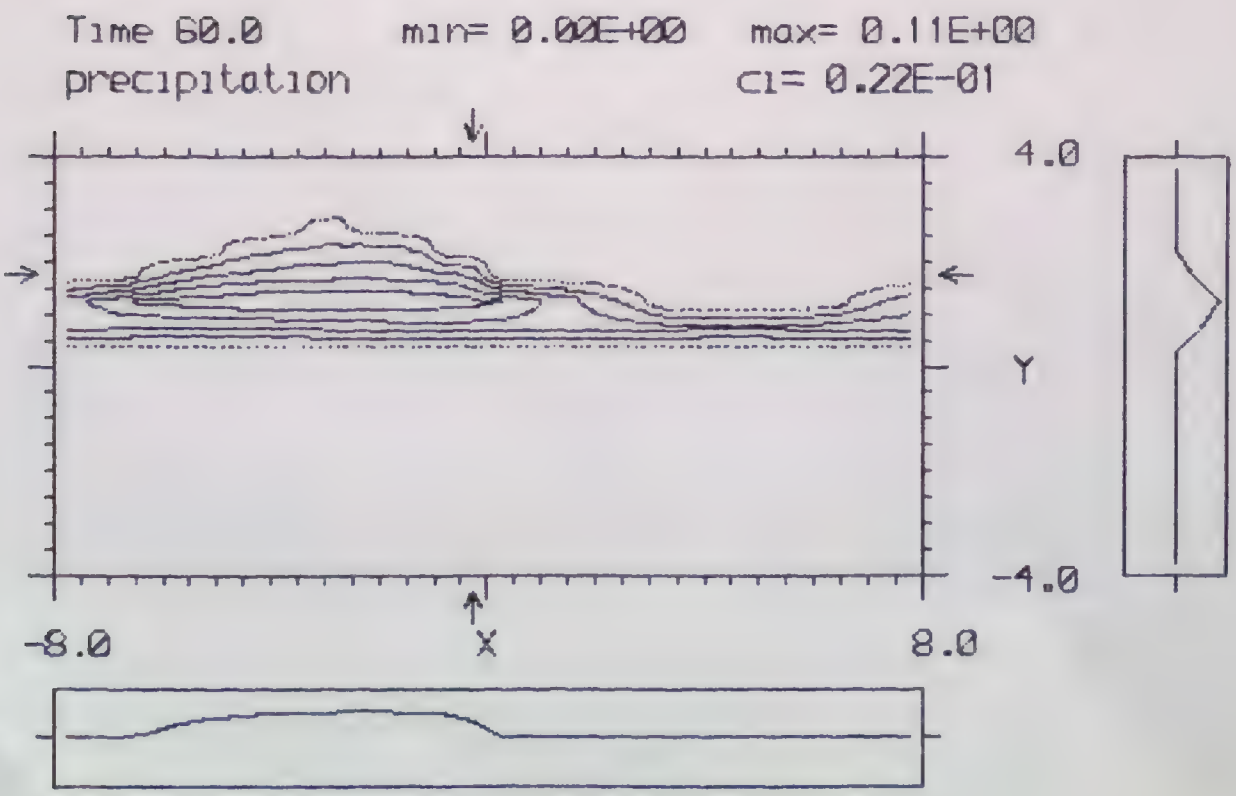

Fig. 6b (July)

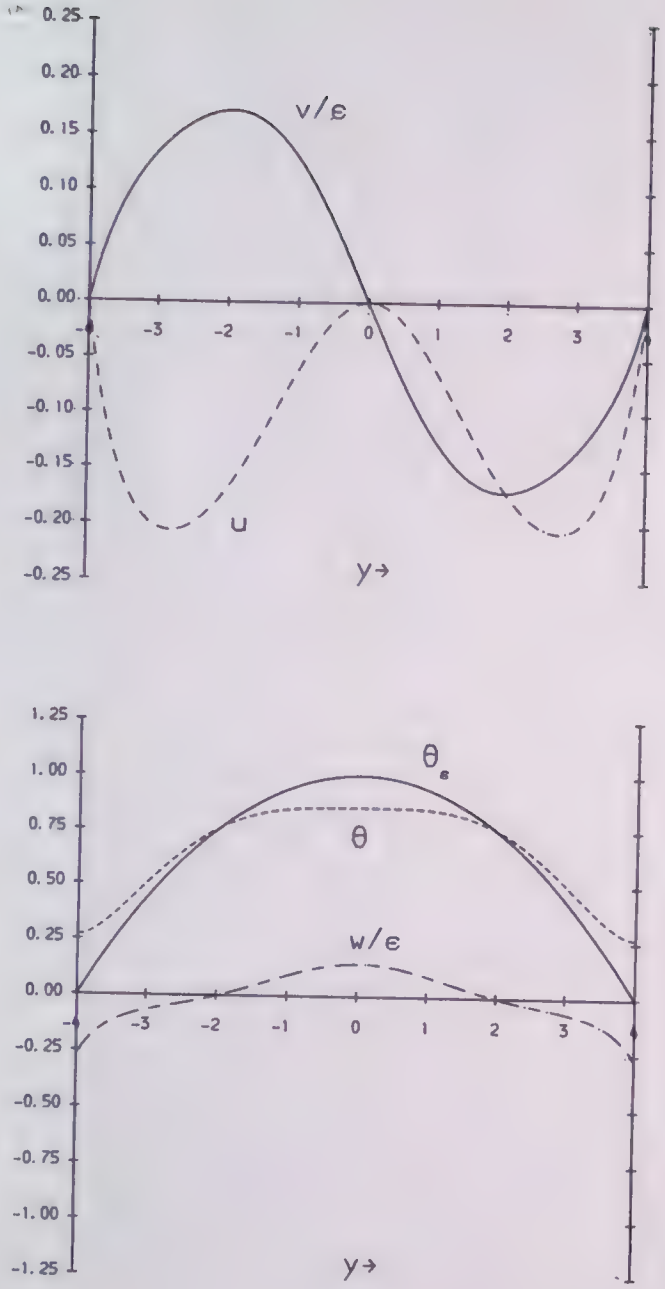
0.25
0.20
0.15
0.10
0.05
0.00
-0.05
-0.10
-0.15
-0.20
-0.25
v/ε
u
y→
-3
-2
-1
0
1
2
3
1.25
1.00
0.75
0.50
0.25
0.00
-0.25
-0.50
-0.75
-1.00
-1.25
θe
θ
w/ε
y→

Fig. 7a

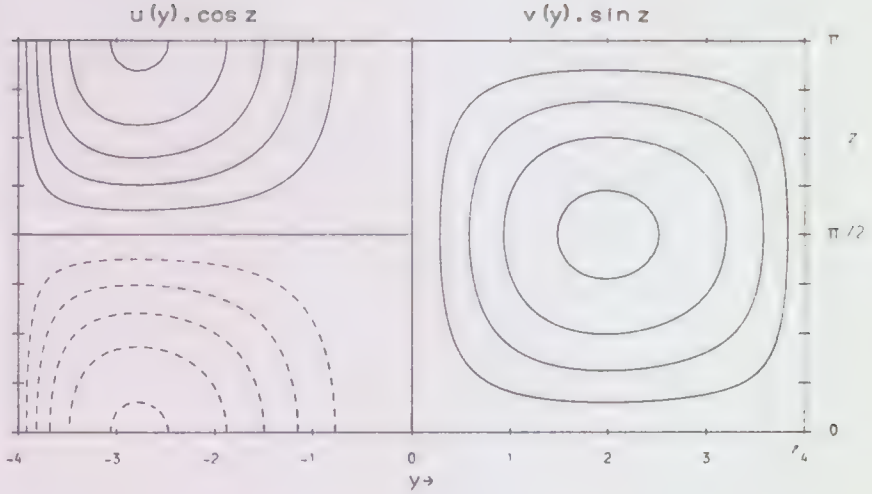
u(y). cos z
v(y). sin z
π
π/2
0
-4
-3
-2
-1
0
1
2
3
π/4
y→

Fig. 7b

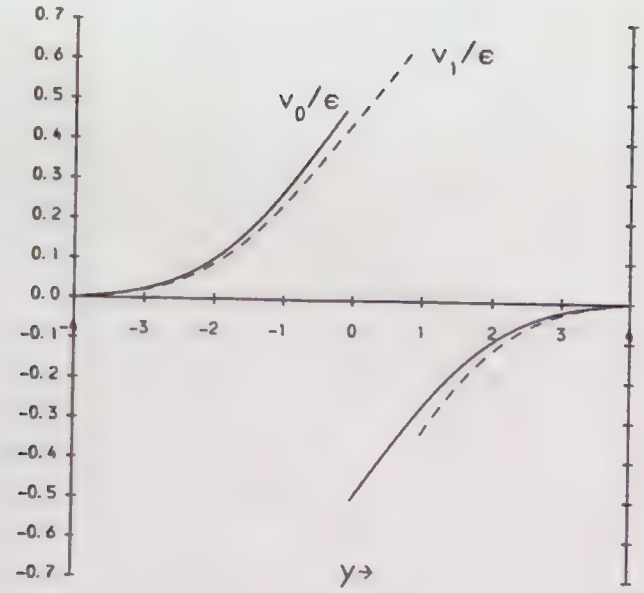
0.7
0.6
0.5
0.4
0.3
0.2
0.1
0.0
-0.1
-0.2
-0.3
-0.4
-0.5
-0.6
-0.7
-3
-2
-1
0
1
2
3
v_0/ϵ
v_1/ϵ
y→

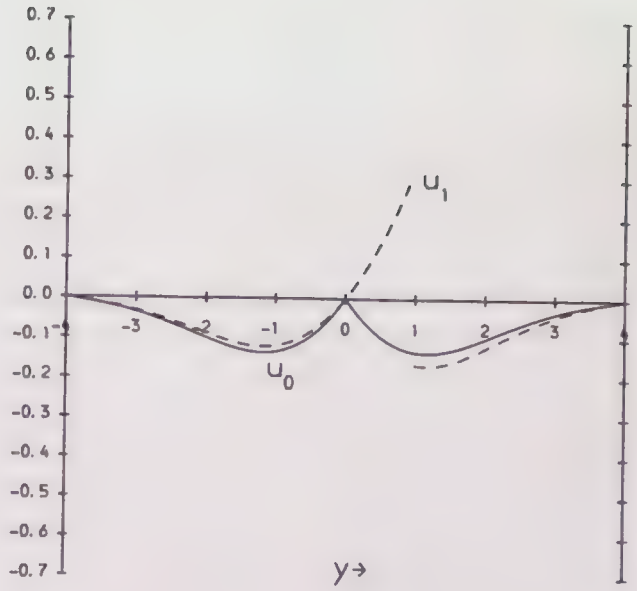
0.7
0.6
0.5
0.4
0.3
0.2
0.1
0.0
-0.1
-0.2
-0.3
-0.4
-0.5
-0.6
-0.7
-3
-2
-1
0
1
2
3
u_1
u_0
y→

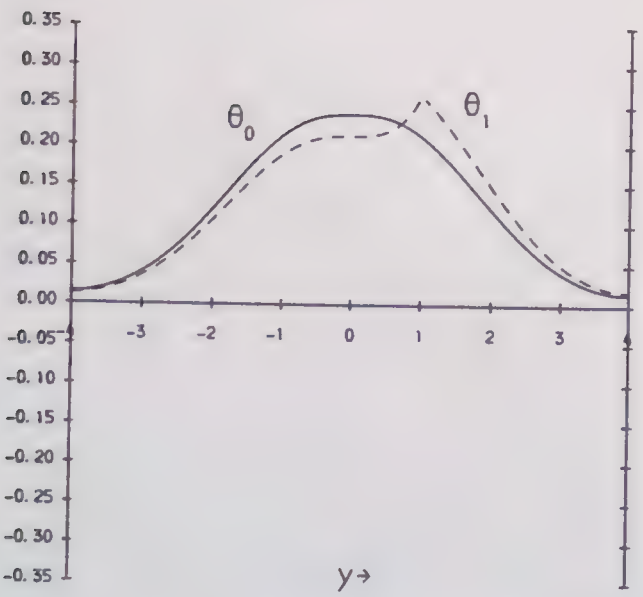
0.35
0.30
0.25
0.20
0.15
0.10
0.05
0.00
-0.05
-0.10
-0.15
-0.20
-0.25
-0.30
-0.35
-3
-2
-1
0
1
2
3
θ_0
θ_1
y→

Fig. 8

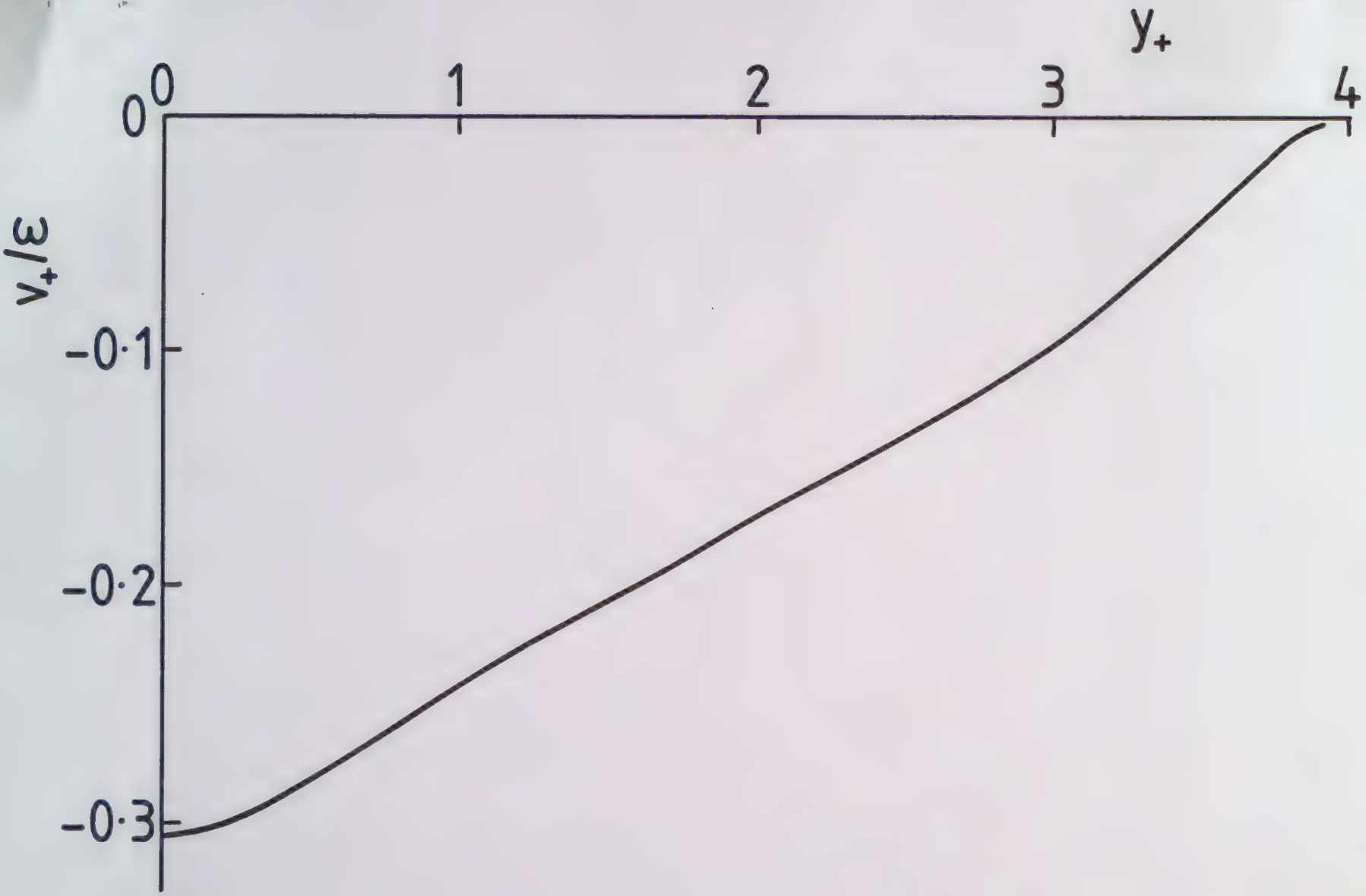

Fig. 9

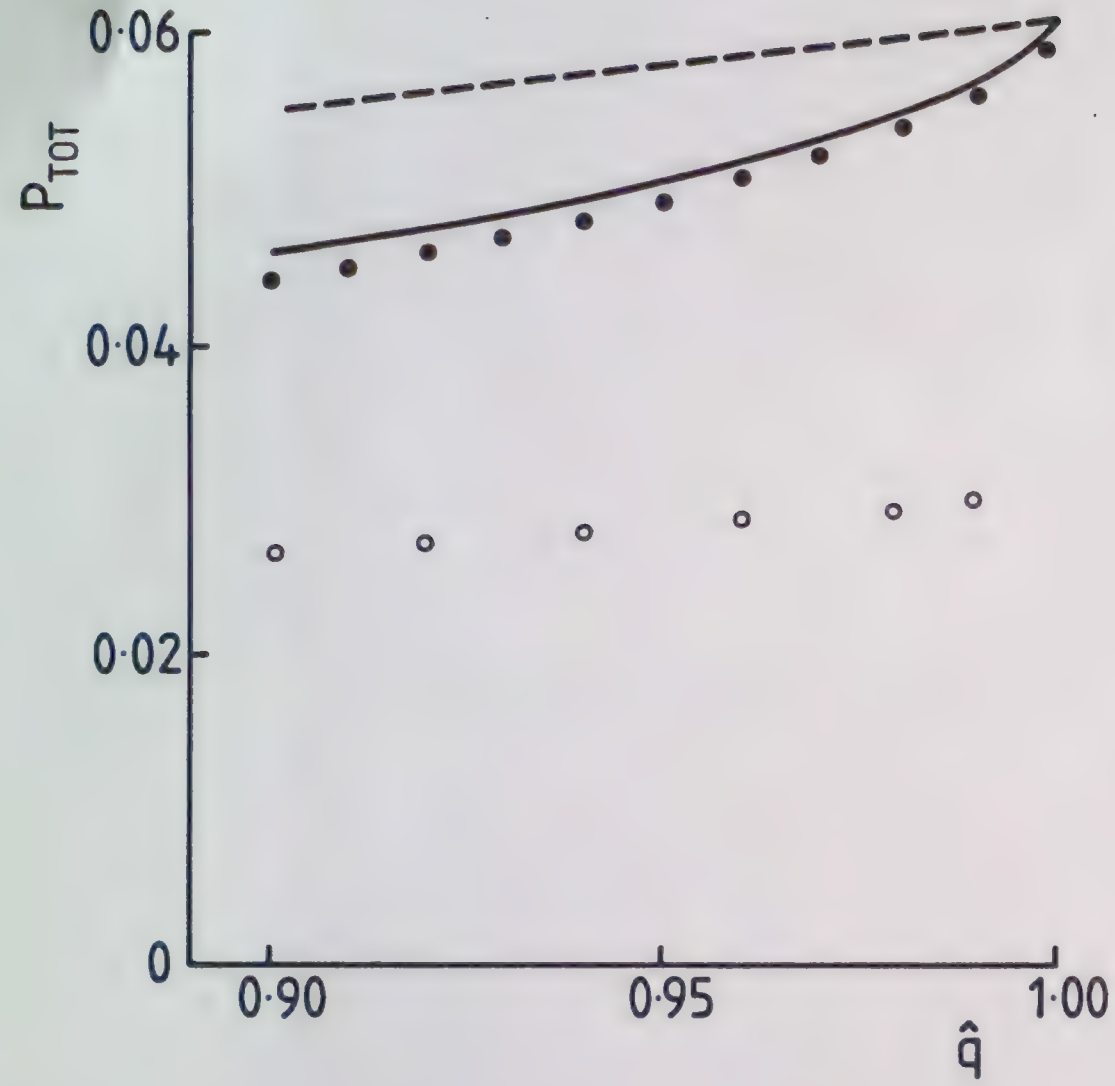

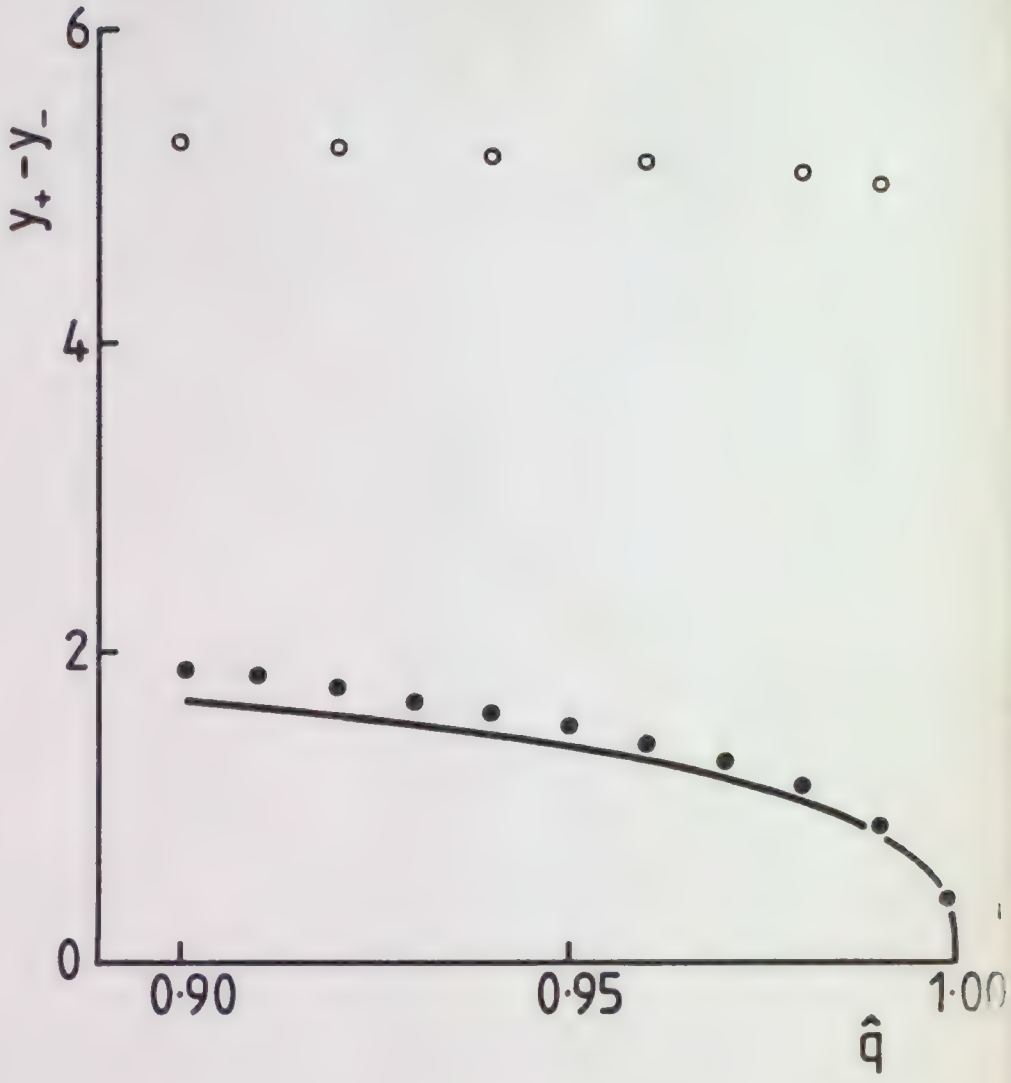

Fig. 10

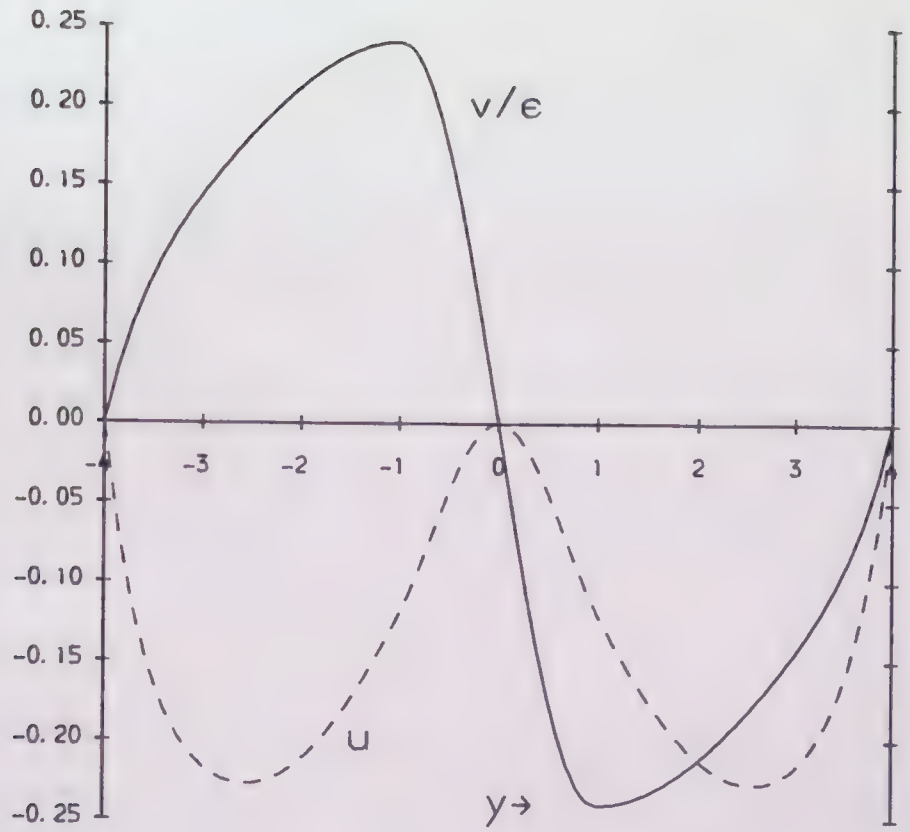
0.25
0.20
0.15
0.10
0.05
0.00
-0.05
-0.10
-0.15
-0.20
-0.25
-4
-3
-2
-1
0
1
2
3
v/ϵ
u
y→

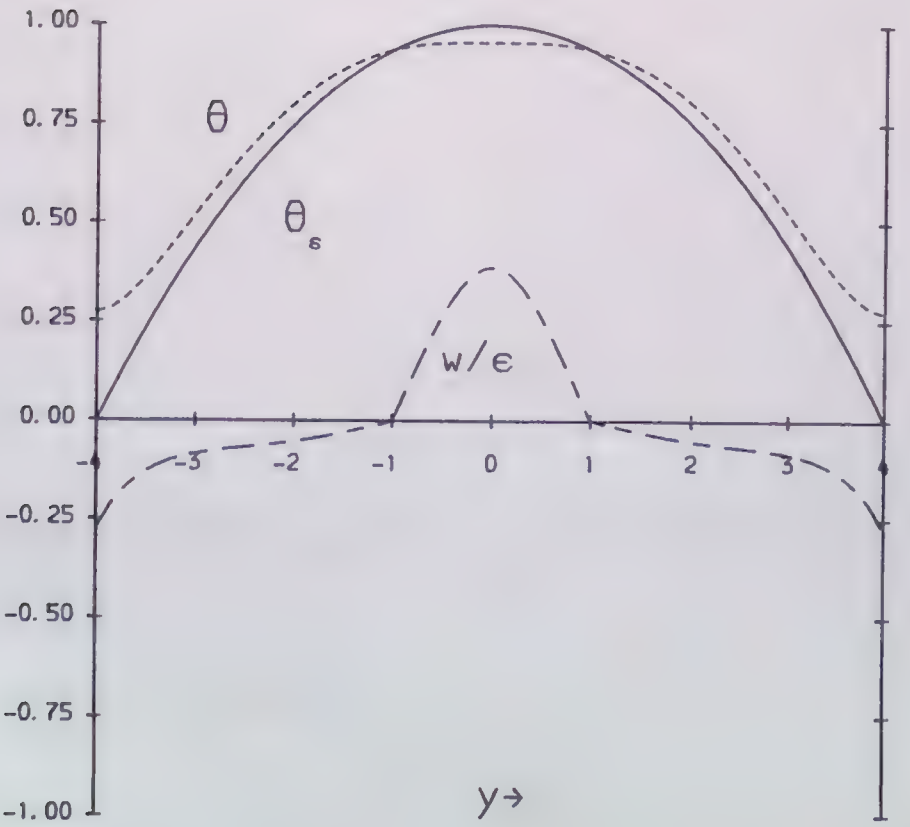
1.00
0.75
0.50
0.25
0.00
-0.25
-0.50
-0.75
-1.00
-4
-3
-2
-1
0
1
2
3
θ
θ_ε
w/ϵ
y→

Fig. 11

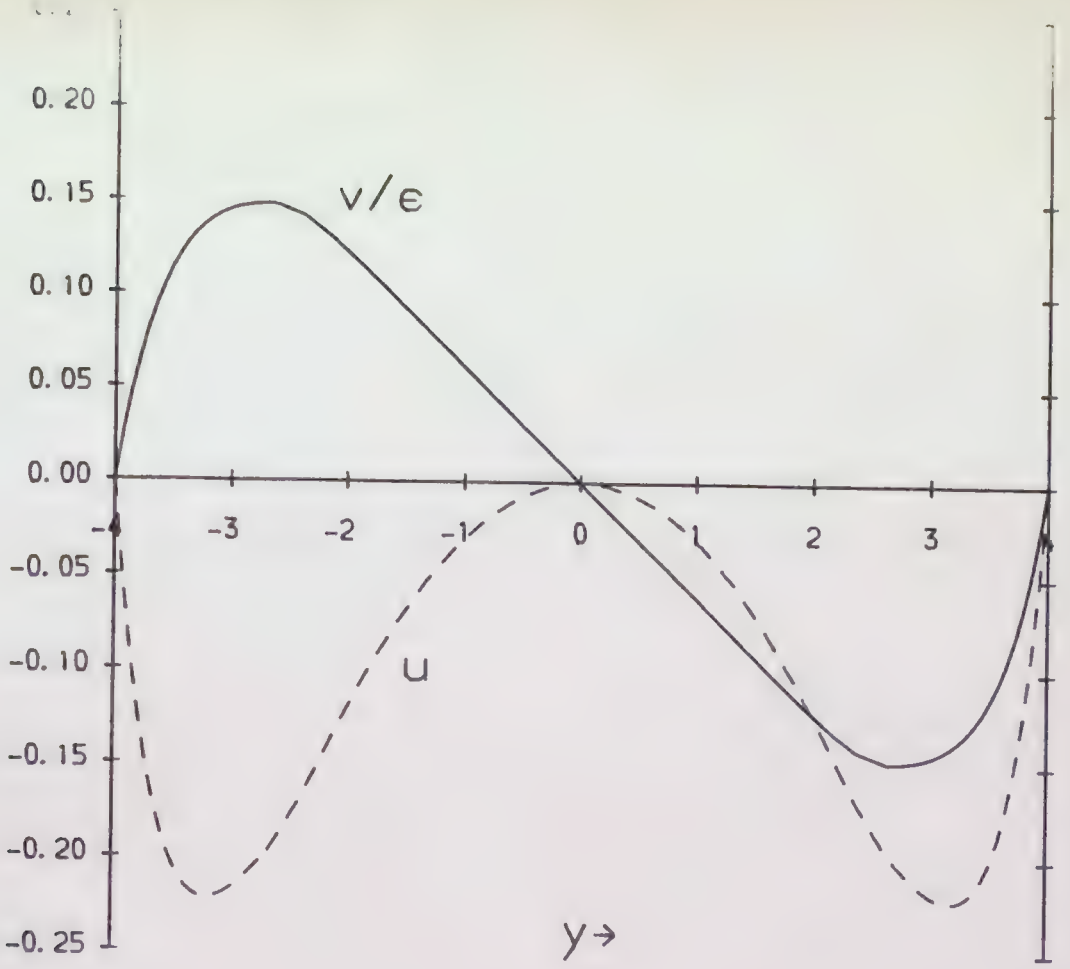
0.20
0.15
0.10
0.05
0.00
-0.05
-0.10
-0.15
-0.20
-0.25
-3
-2
-1
0
1
2
3
v/ε
u
y→

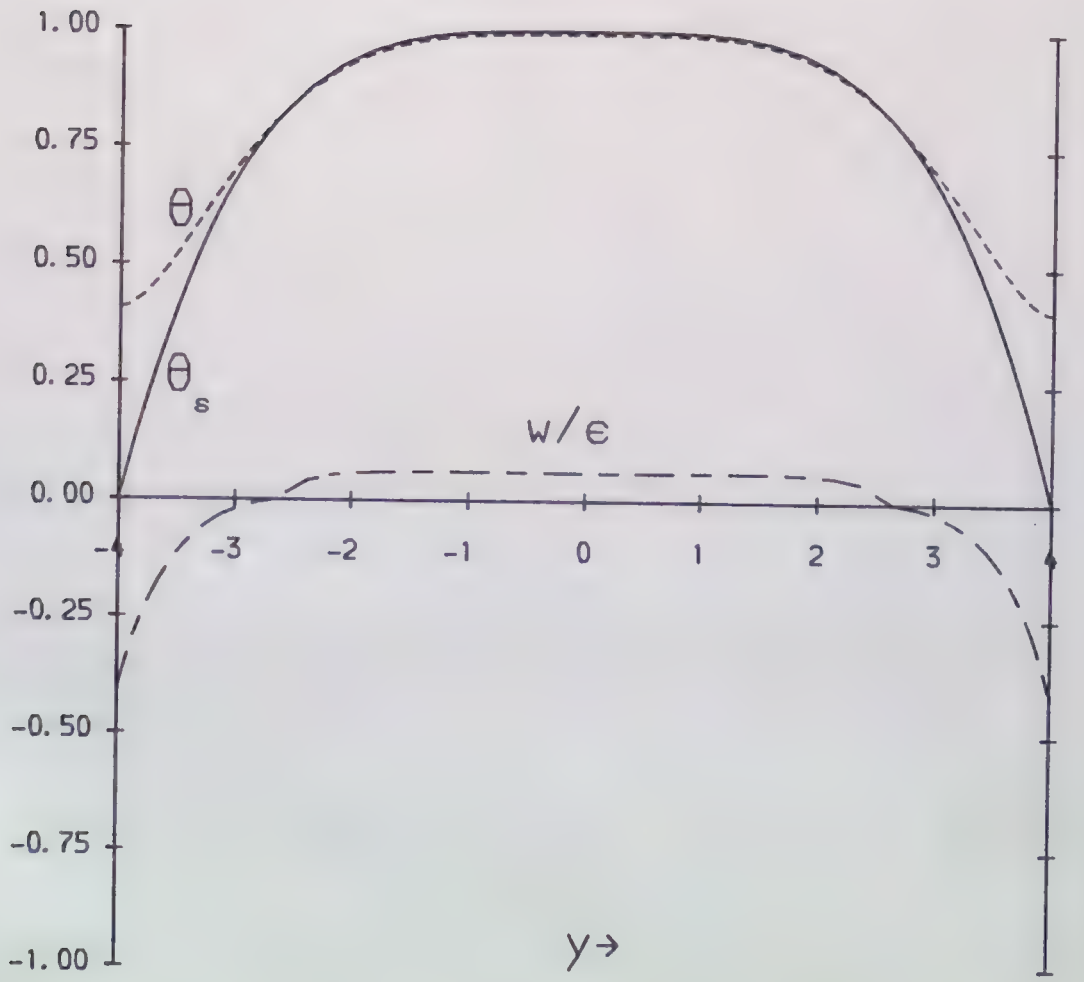
1.00
0.75
0.50
0.25
0.00
-0.25
-0.50
-0.75
-1.00
-3
-2
-1
0
1
2
3
θ
θs
w/ε
y→

Fig. 12

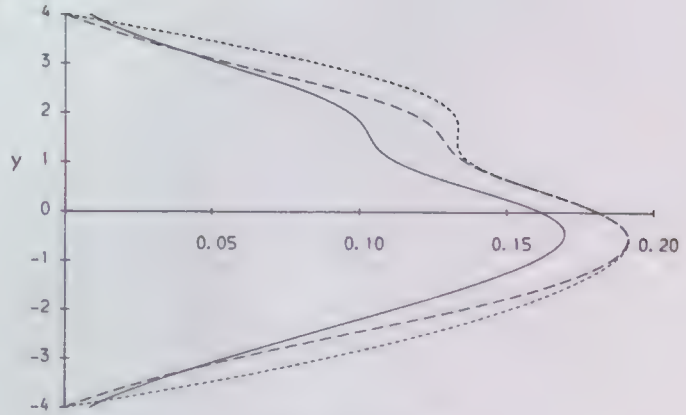

Amplitude of w'/ε

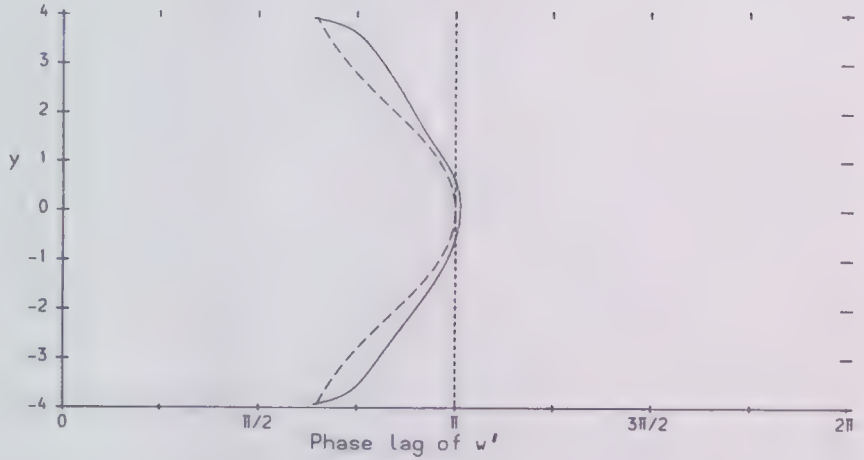

Phase lag of w'

Fig. 13a

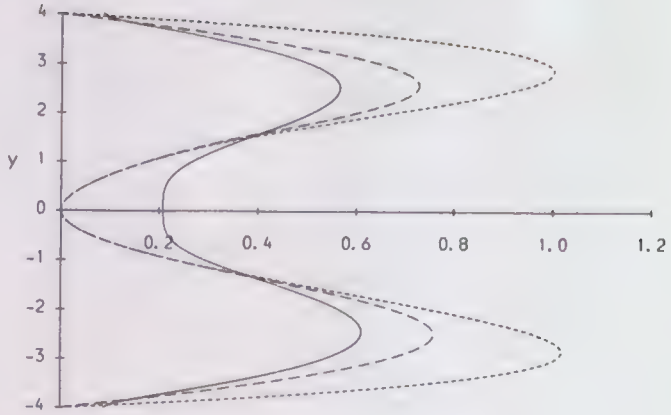

Amplitude of θ'/ε

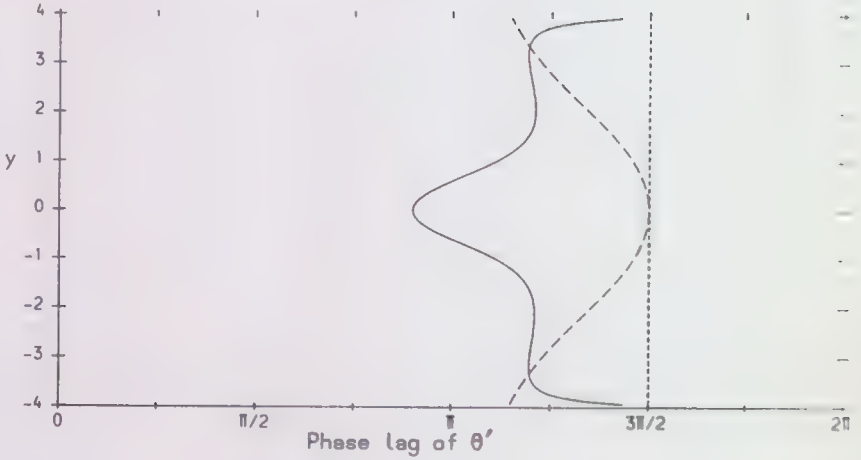

Phase lag of θ'

Fig. 13 b

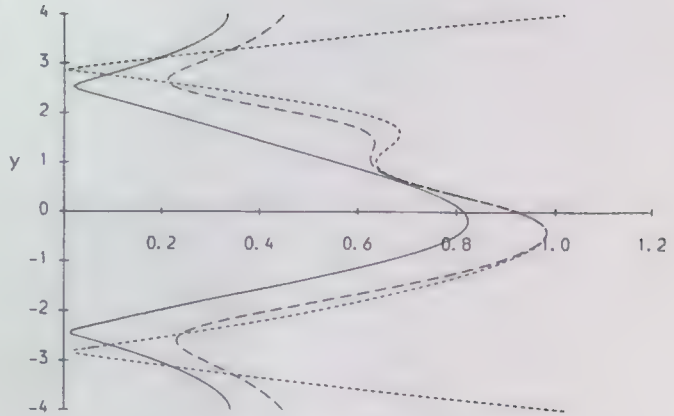

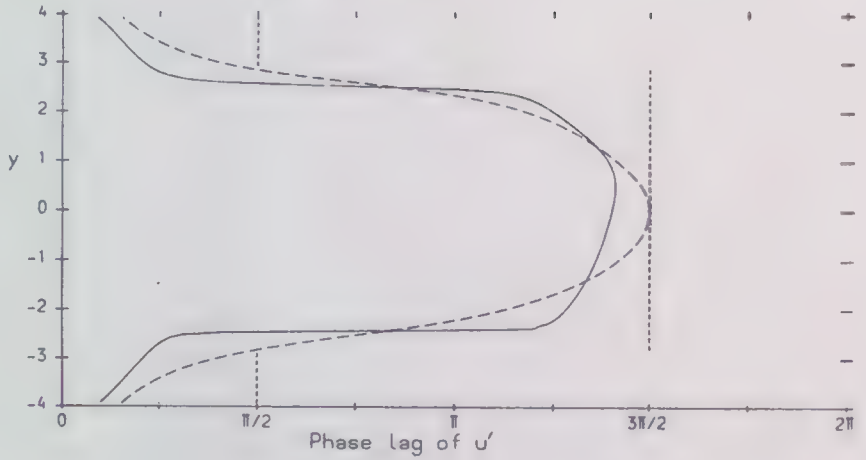

Fig. 13c

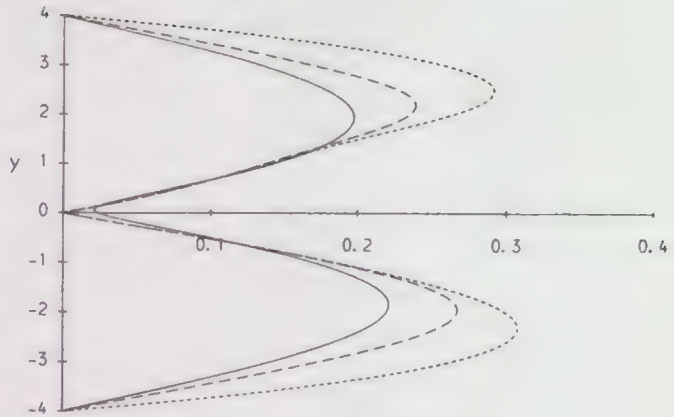

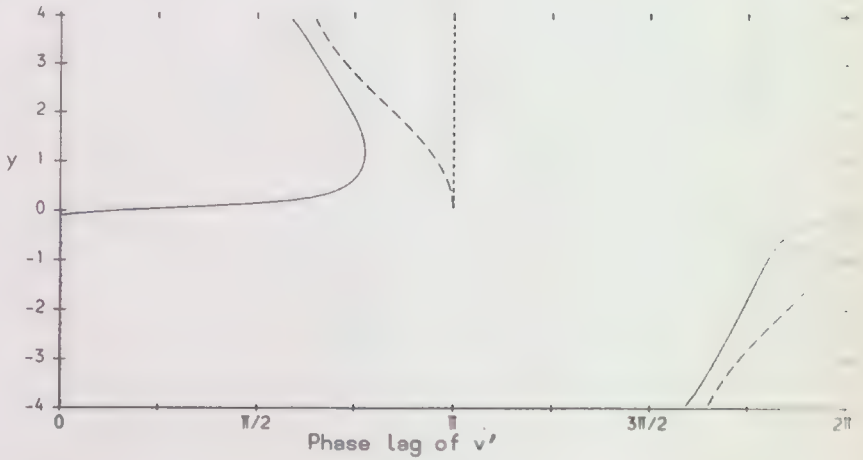

Fig. 13d

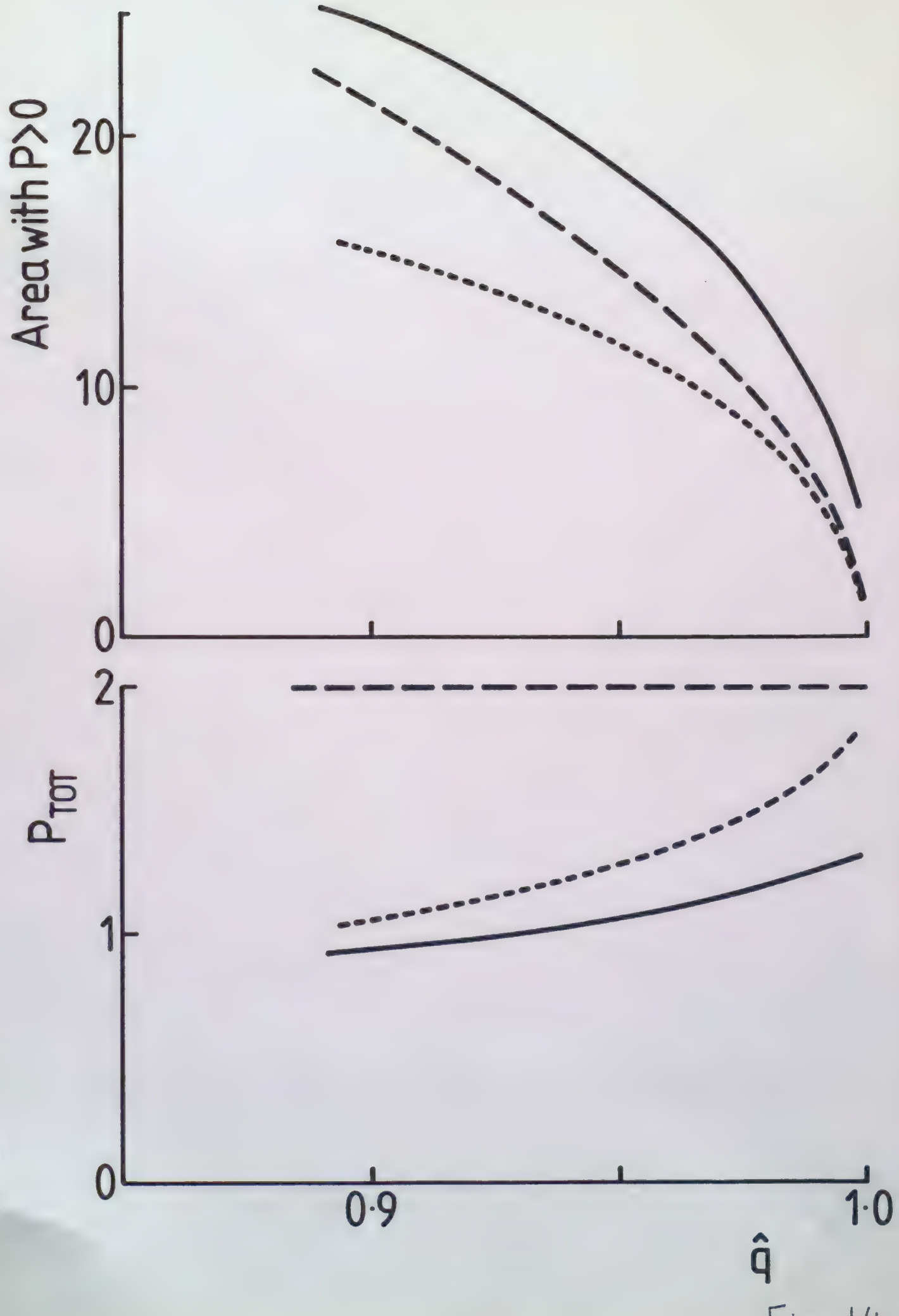

Fig. 14

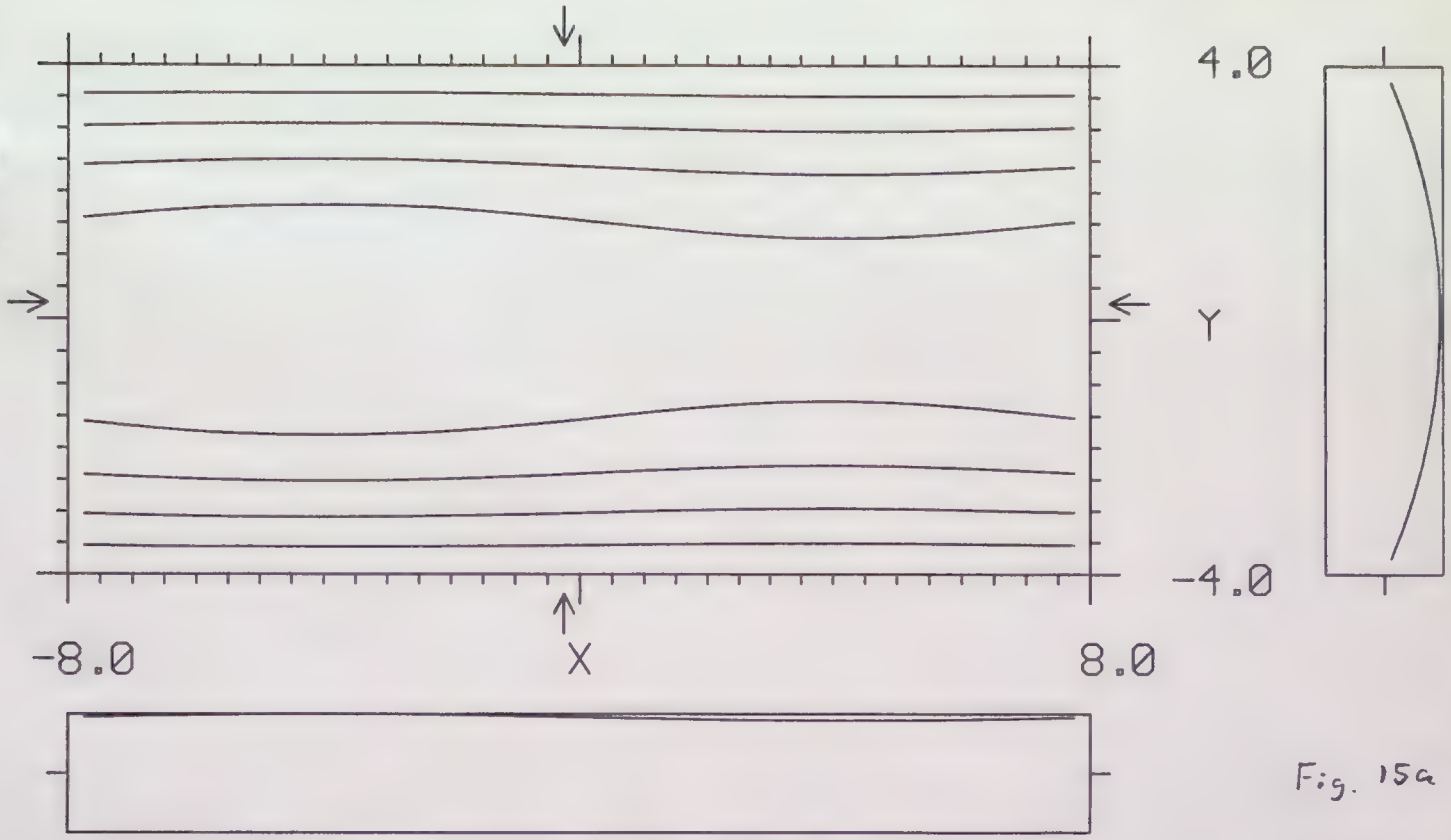

Fig. 15a

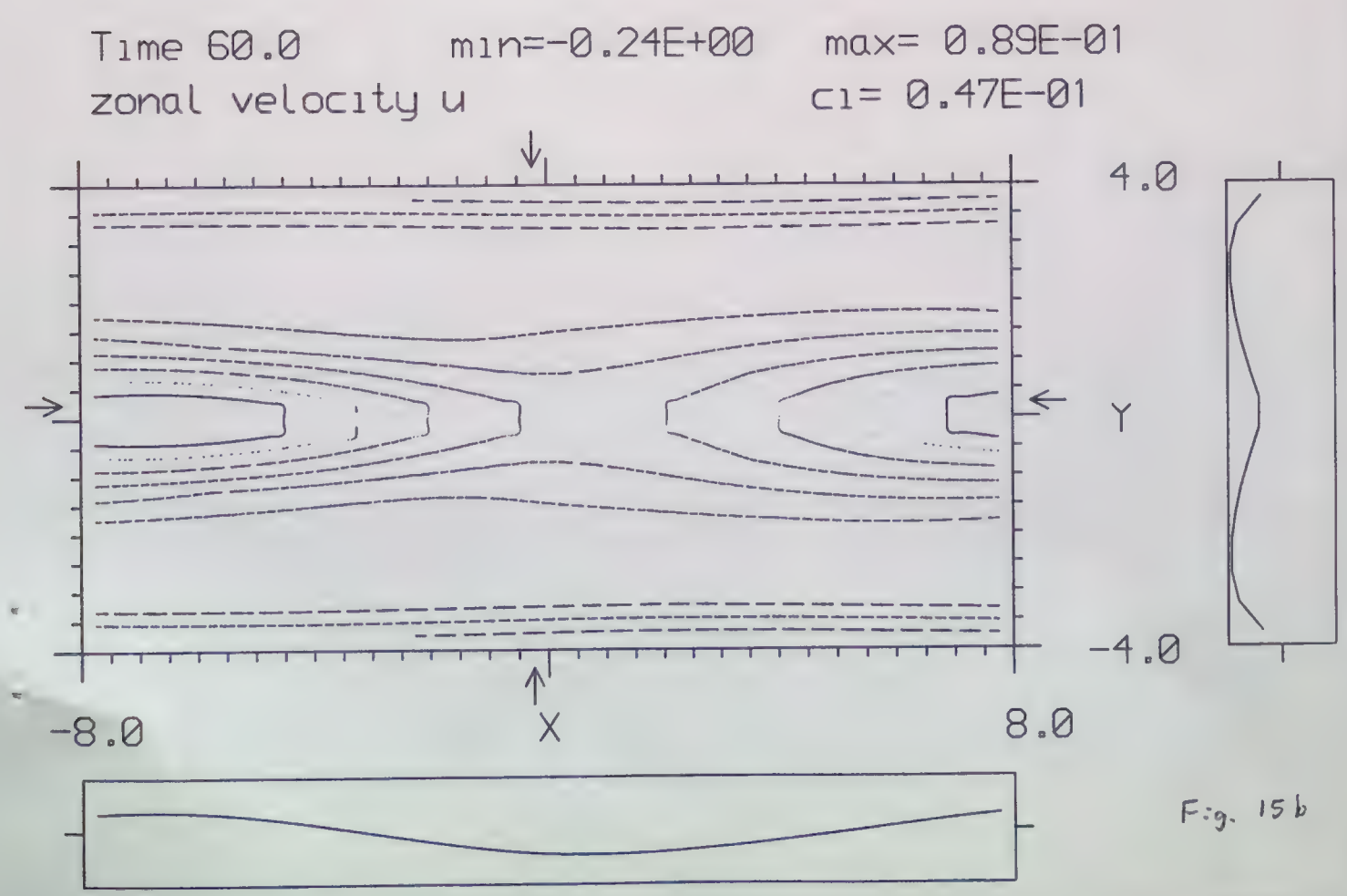

Fig. 15b

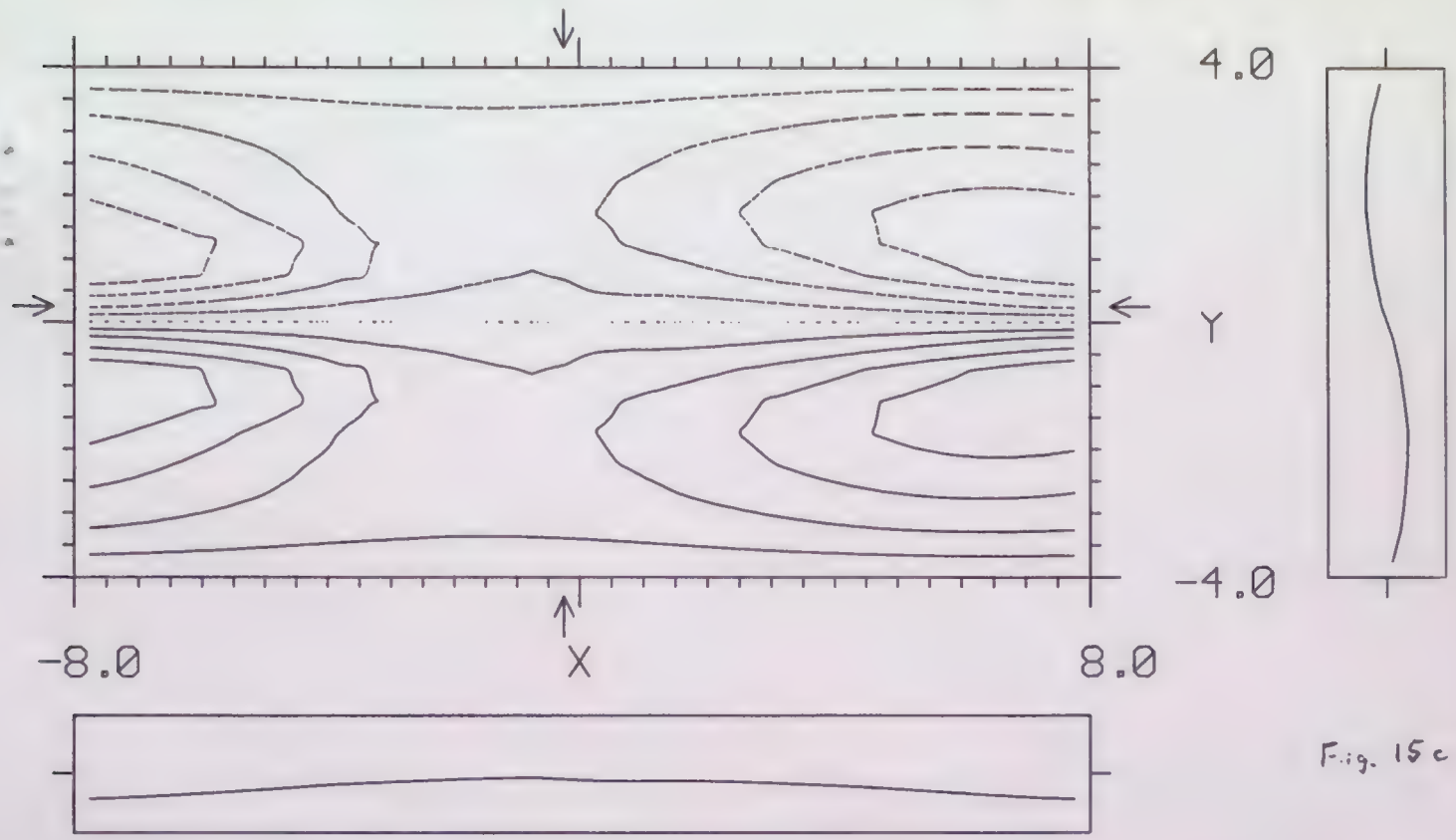

Fig. 15c

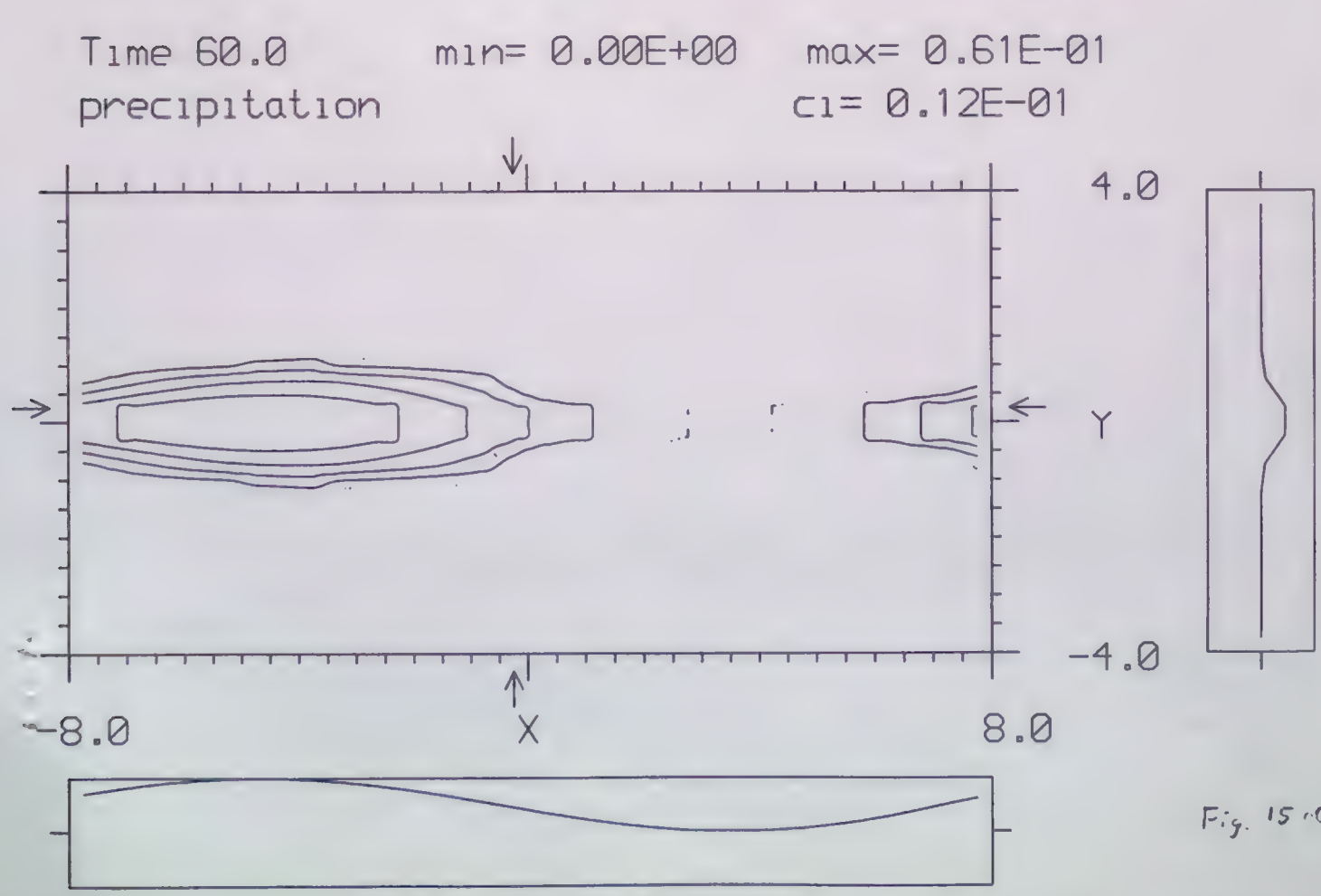

Fig. 15d

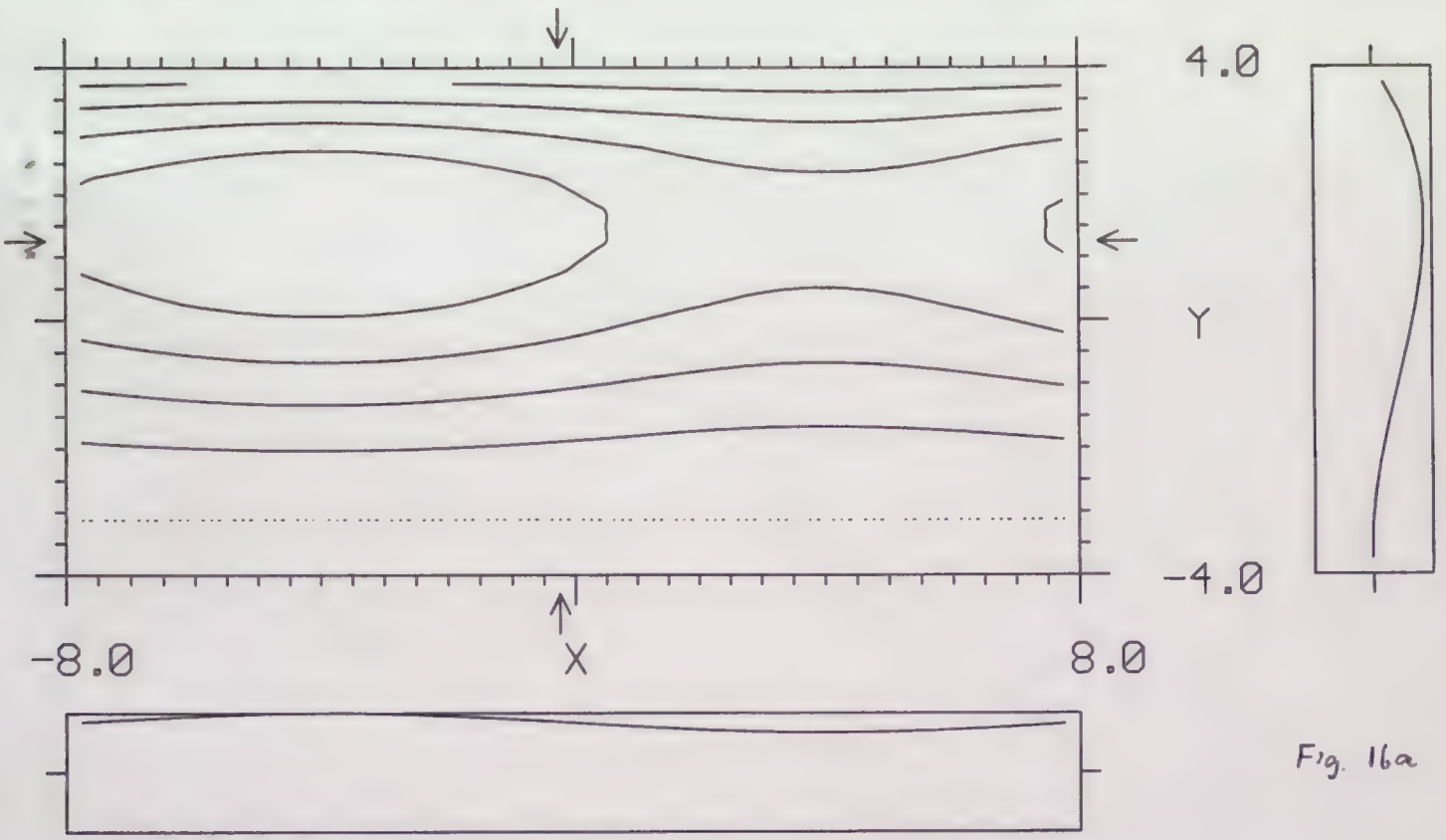

Fig. 16a

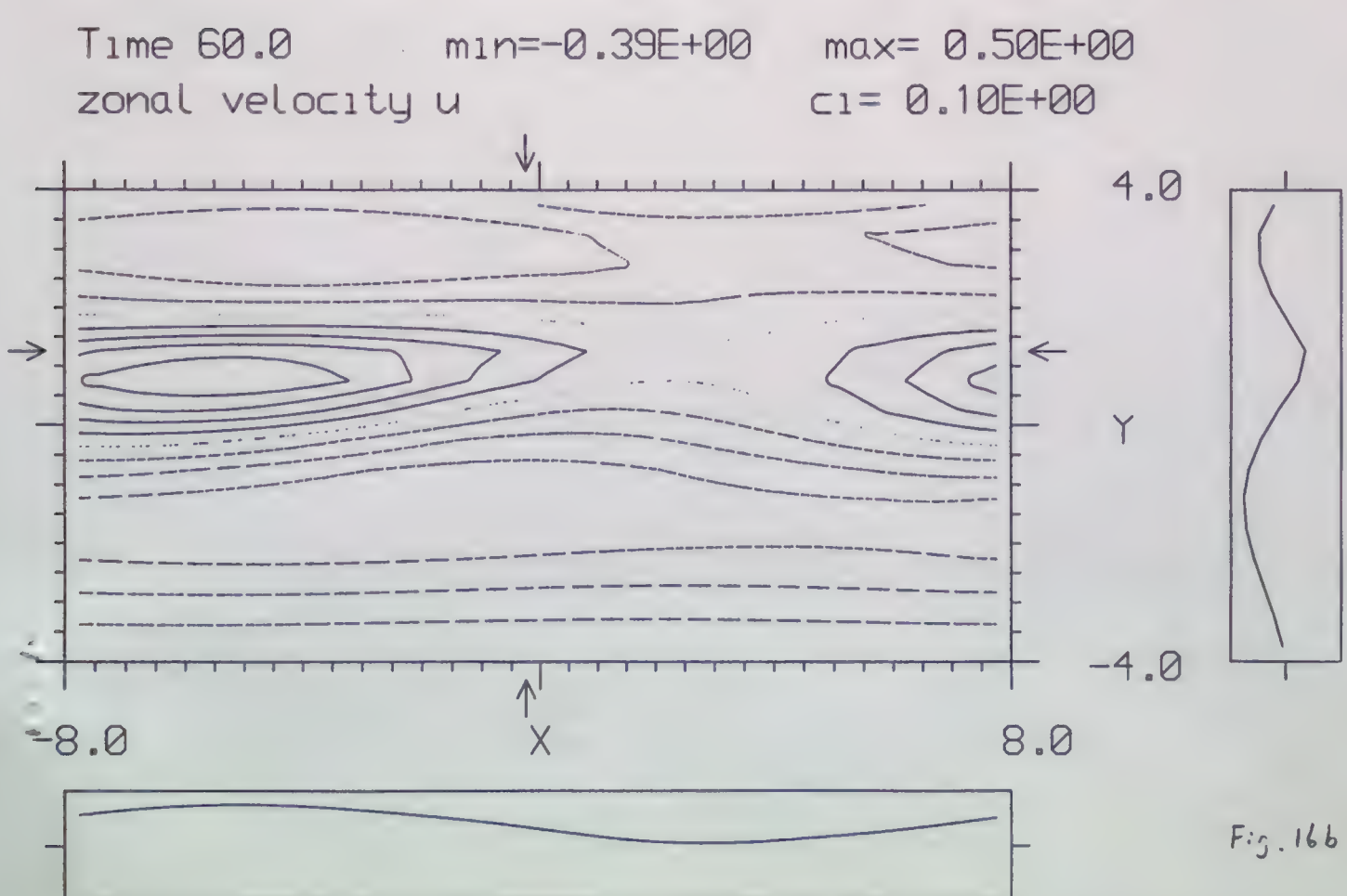

Fig. 16b

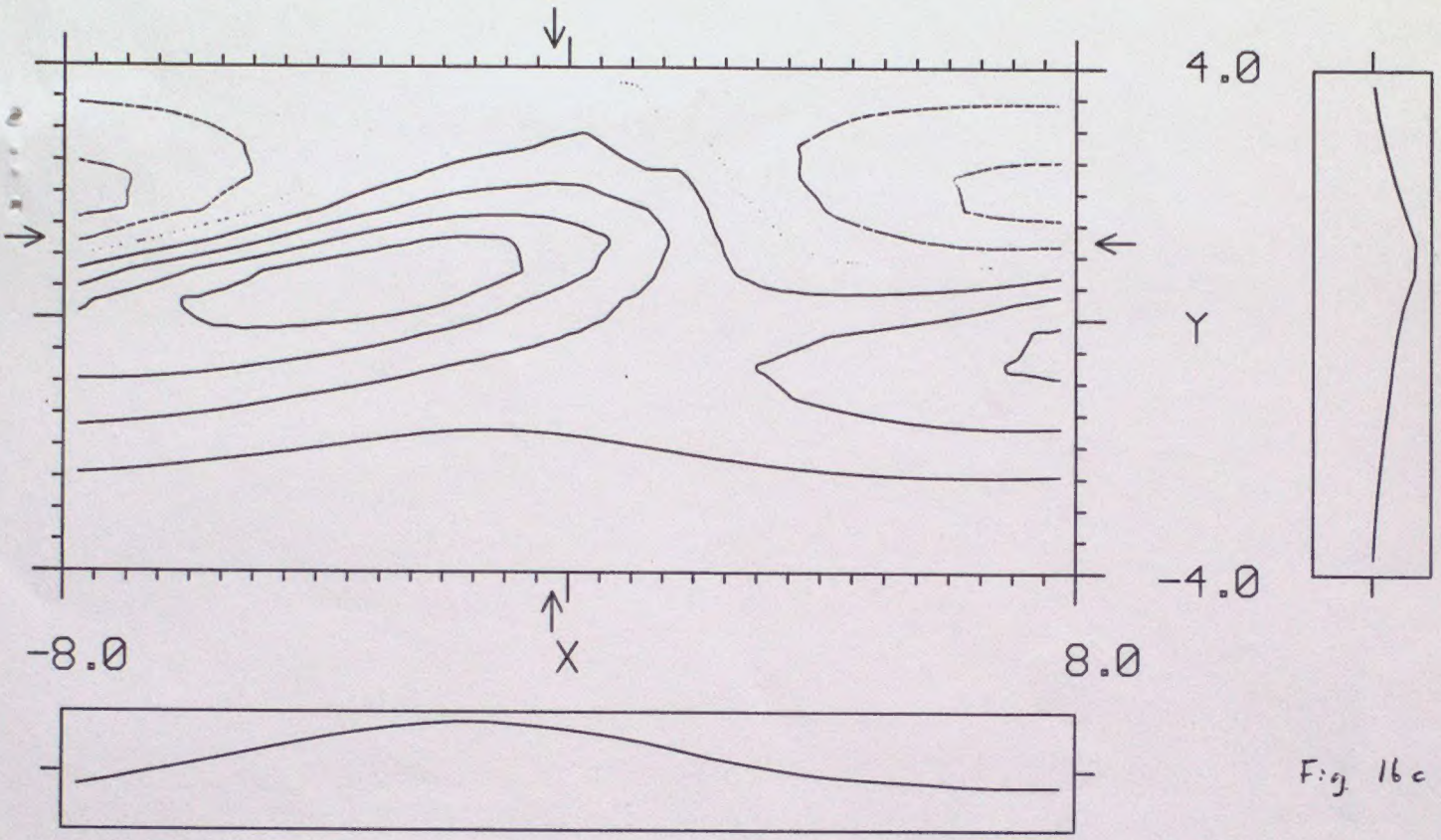

Fig. 16c

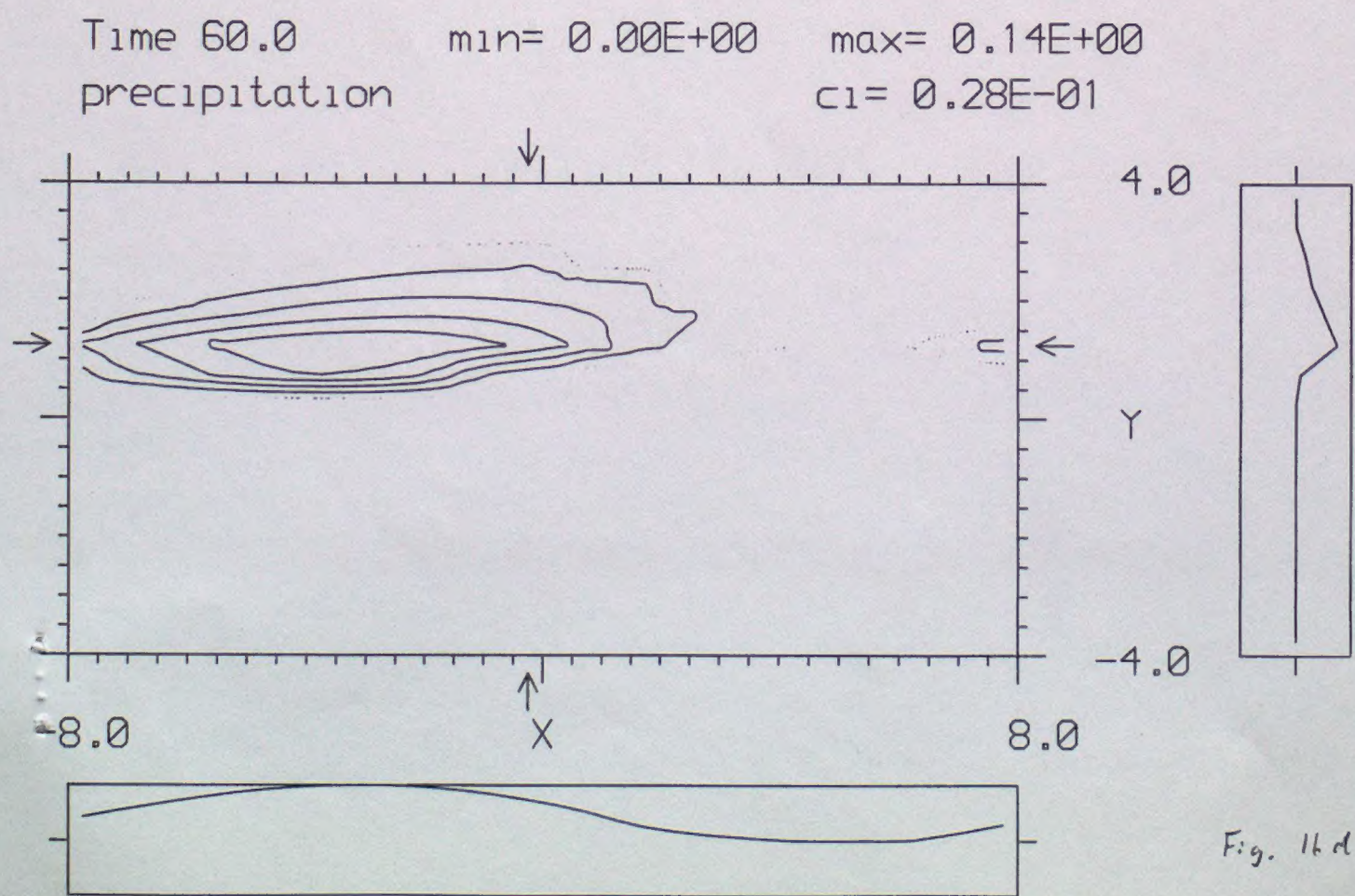

Fig. 16d

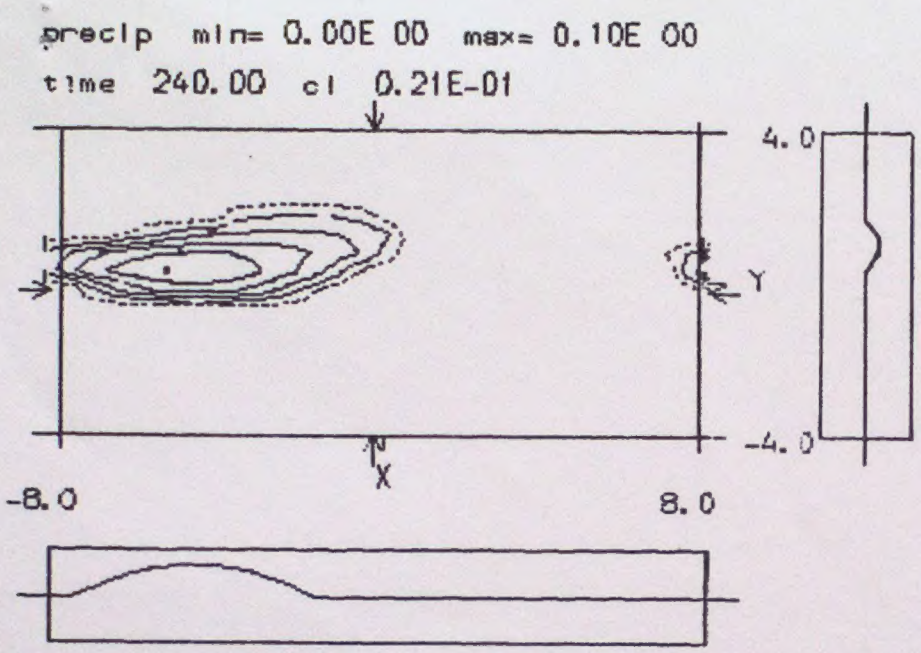

Fig. 17a

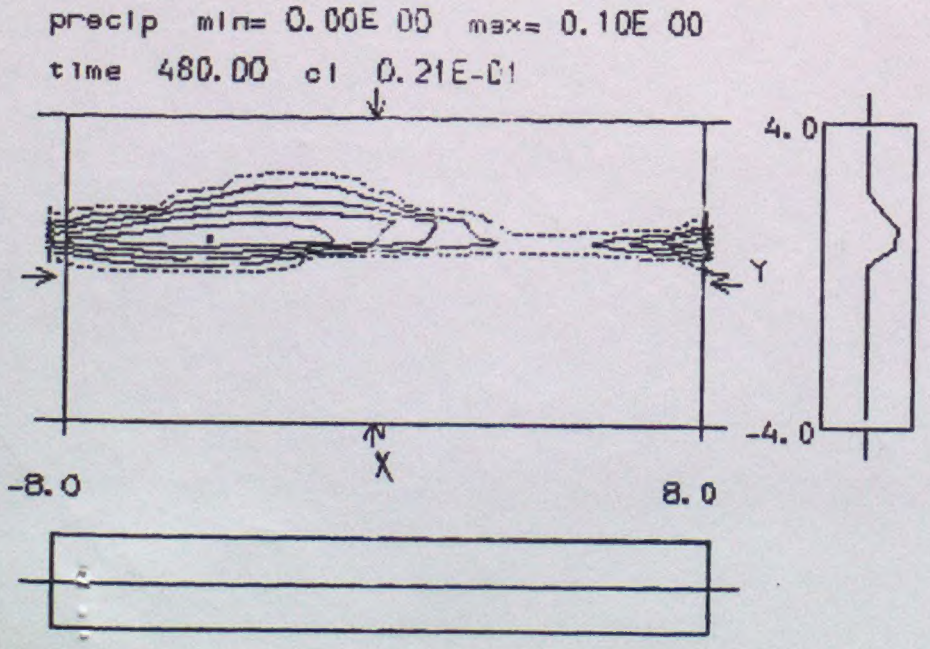

Fig. 17b

DYNAMICAL CLIMATOLOGY TECHNICAL NOTES

DCTN 1 June 1984
A scheme for incorporating the thermodynamic sea-ice model into a coupled ocean-atmosphere model.
C Gordon and M Bottomley

DCTN 2 Sept 1984
The parametrization of the upper ocean mixed layer in coupled ocean/atmosphere models.
C Gordon and M Bottomley

DCTN 3 Sept 1984
The response of a simple thermodynamic sea-ice model to GCM forcing appropriate for perennial sea-ice.
M Bottomley

DCTN 4 Sept 1984
Potential vorticity in the stratosphere derived using data from satellites.
S A Clough, N S Grahame and A O'Neill

DCTN 5 Sept 1984
Simulation of the seasonal cycle of SST using globally specified climatological data to force simple ocean models.
N S Grahame

DCTN 6 Sept 1984
Development of an improved GCM radiation scheme.
A Slingo and R C Wilderspin

DCTN 7 Sept 1984
On the specification of surface fluxes in coupled atmosphere/ocean general circulation models.
J F B Mitchell, C A Wilson and C M Price

DCTN 8 Sept 1984
A survey of possible repercussions of the Soviet river reversal programme on Arctic sea-ice.
H Cattle

DCTN 9 Oct 1984
A study of a strong stratospheric warming during January 1982
T D A Fairlie

DCTN 10 Nov 1984
An intercomparison of the Met O 11 N45 model and the Met O 20 11-level model on the Cyber 205
J F Dyson

DCTN 11 Nov 1984
Simulation of observed time series of temperature and precipitation over eastern England.
D N Reed

DCTN 12 Nov 1984
Forecasts and analyses of the onset of the Southwest monsoon.
R Kershaw

DCTN 13 Nov 1984
On modelling the effects of CO_2 on climate.
J F B Mitchell

DCTN 14 Dec 1984
Development of a revised longwave radiation scheme for an atmospheric general circulation model.
A Slingo and R C Wilderspin

DCTN 15 Jan 1985
Rossby wavetrains in the stratosphere forced by localised disturbances in the troposphere.
C J Marks (Oxford), A O'Neill and V D Pope

DYNAMICAL CLIMATOLOGY TECHNICAL NOTES

DCTN 16 Jan 1985
Observing system experiments using the Meteorological Office's 15-level model.
R A Bromley

DCTN 17 Feb 1985
Atmospheric general circulation simulation of the climate of the Mediterranean region.
H Cattle

DCTN 18 Feb 1985
Diurnal variation and cloud in a general circulation model.
C A Wilson and J F B Mitchell

DCTN 19 Feb 1985
The sensitivity of the Saharan region in a general circulation model.
W M Cunnington and P R Rowntree

DCTN 20 Mar 1985
The impact of aircraft observations on analyses and forecasts from the operational 15-level model.
B R Barwell

DCTN 21 Mar 1985
Non-linear effects on heat-induced circulation of the tropical atmosphere.
A E Gill and P J Phlips

DCTN 22 Apr 1985
Simulation of cloudiness with the U.K. Meteorological Office 11-layer AGCM.
A Slingo and R C Wilderspin

DCTN 23 Apr 1985
An integrated approach to the representation of cloud processes. R N B Smith

DCTN 24 May 1985
Nuclear Winter: Calculations of the shortwave radiative effects of soot aerosols.
A Slingo and P Goldsmith

DCTN 25 Jul 1985
Sea ice and the Antarctic winter circulation: a numerical experiment.
J F B Mitchell and T S Hills

DCTN 26 Jul 1985
A Budyko-Sellers model for study of ocean-atmosphere interaction.
W J Ingram

DCTN 27 Aug 1985
The effect of a shoaling thermocline on equatorially-trapped Kelvin waves.
A E Gill and B A King

DCTN 28 Sept 1985
CO_2 climate sensitivity and model dependence of results.
J F B Mitchell, C A Wilson and W M Cunnington

DCTN 29 Sept 1985
Handbook of the Meteorological Office 11-layer atmospheric general circulation model.
Volume 1 : Model Description
Edited by A Slingo

DCTN 30 Sept 1985
Impact of land surface variations on African rainfall in general circulation models.
P R Rowntree, M F Wilson and A B Sangster

DYNAMICAL CLIMATOLOGY TECHNICAL NOTES

DCTN 31	Nov 1985	The annual cycle of sea level in the eastern tropical Pacific. G R Bigg and A E Gill
DCTN 32	Nov 1985	An analytic model of the heat-induced tropical circulation in the presence of a mean wind. P J Phlips and A E Gill
DCTN 33	Nov 1985	The effect of resolution and diffusion on the simulated climate. J F Dyson
DCTN 34	Jan 1986	Rossby adjustment over a step. M K Davey, A E Gill, E R Johnson and P F Linden
DCTN 35	Jan 1986	Issues concerning the evaluation of effective surface roughness of heterogeneous terrain. D J Carson
DCTN 36	Mar 1986	Climate sensitivity and past climates : evidence from numerical studies J F B Mitchell
DCTN 37	Mar 1986	Parametrizations of land-surface processes in Meteorological Office numerical weather prediction and climate models D J Carson
DCTN 38	Apr 1986	Modelling of land-surface processes and their influence on European Climate D A Warrilow, A B Sangster and A Slingo
DCTN 39	Apr 1986	Simulation of climatic change due to increased CO_2 J F B Mitchell
DCTN 40	May 1986	On the interpretation of the Eliassen-Palm flux divergence. **Part I :** Theory D G Andrews
DCTN 41	June 1986	Experiments on tropical circulation with a simple moist model. M K Davey and A E Gill
DCTN 42	Jun 1986	Parameter regimes for studying isolated eddies. P D Killworth and M K Davey